

# Search for Heavy Neutral Leptons with IceCube DeepCore

Dissertation  
zur Erlangung des akademischen Grades  
doctor rerum naturalium  
(Dr. rer. nat.)

im Fach: Physik  
Spezialisierung: Experimentalphysik

eingereicht an der  
Mathematisch-Naturwissenschaftlichen Fakultät  
der Humboldt-Universität zu Berlin

von  
**Leander Fischer M. Sc.**  
geboren am 24. Oktober 1992  
in Heidelberg

Präsidentin der Humboldt-Universität zu Berlin  
Prof. Dr. Julia von Blumenthal

Dekanin der Mathematisch-Naturwissenschaftlichen Fakultät  
Prof. Dr. Caren Tischendorf

### **Copyright Notice**

This book is released into the public domain using the CC-BY-4.0 code.

To view a copy of the CC-BY-4.0 code, visit:

<https://creativecommons.org/licenses/by/4.0/>

### **Colophon**

This document was typeset with the help of KOMA-Script and L<sup>A</sup>T<sub>E</sub>X using the open-source kaobook template class.

The source code of this thesis is available at:

[https://github.com/LeanderFischer/phd\\_thesis](https://github.com/LeanderFischer/phd_thesis)

## **Zusammenfassung**

Zusammenfassung ...

## **Abstract**

Abstract ...



# Todo list

adjust final vertical position of this reference . . . . .	1
Also cite this? Didn't find a good reference, only the press releases. . . . .	1
Introduce SM EW NC/CC Lagrangian to build upon in the next chapter . . . . .	3
Plot is missing + for W and 0 for Z boson. . . . .	3
Cite and/or sidenote this. . . . .	4
cite this . . . . .	4
cite neutrino oscillations/flavor conversions . . . . .	4
namedrop RH=sterile=HNL and why they are called like this based on the SM EW Lagrangian introduced above . . . . .	4
write some interlude to motivate atm. neutrinos as source for HNL searches/production etc. . . . .	6
Say something about atmospheric neutrino flux uncertainties, based on recent JP/Anatoli papers. . . . .	7
add current BF values from nufit or so? . . . . .	9
say something about how this changes with matter . . . . .	10
Re-write/re-formulate this section (copied from HNL technote). . . . .	10
Produce similar styled plot for these limits . . . . .	10
This section really needs to be re-written to motivate the search for HNLs from a more generic point of view (e.g. to explain neutrino masses) . . . . .	11
This section definitely needs to be elaborated in a little more detail . . . . .	11
Not adding information about the case where the neutrinos have Dirac or pseudo-Dirac masses . . . . .	12
maybe I want a figure for this, or not so important? (YELLOW) . . . . .	15
Elaborate whether this is the case (show it in a plot?). Discuss directionality of cascades in general. (ORANGE) . . . . .	15
fix caption of this figure (RED) . . . . .	16
fix caption of this figure (RED) . . . . .	17
Describe the results plots here for the first time, so I can come back to the observed features later? Or maybe drop them and just show them later? (RED) . . . . .	18
From HNL Note, re-write/change (RED) . . . . .	21
describe the "good fit" selection when I first show plots that use it (ORANGE) . . . . .	22
add some 1D resolution plots (ORANGE) . . . . .	22
fix caption of this figure (RED) . . . . .	22
fix caption of this figure (RED) . . . . .	22
fix caption of this figure (RED) . . . . .	23
fix caption of this figure (RED) . . . . .	24
fix caption of this figure (RED) . . . . .	24

Make plot to show efficiency of the OscNext selection for HNL events. (ORANGE) . . . . .	25
add information about the matter profile used (ORANGE) . . . . .	27
add information about the oscillation probability calculation and the software used for it (RED) . . . . .	27
Should I adapt the total numbers to match the sum of the rounded individual parts? (YELLOW) . . . . .	27
add 3D expectation and/or S/sqrt(B) plots . . . . .	28
Add fractions of the different particle types in the bins for benchmark mass/mixing (another table)? (ORANGE) . . . . .	28
Do I want more information about the different pipelines and stages? Could link back to the extra stage I wrote and add the earth model and oscillation calculation information here, I guess?! (ORANGE)	28
I feel like I have to be a bit more precise on what is the fit metric (e.g. the mod chi2) and what is the TS, as in the mod chi2 difference, which is the actual TS, right? (RED) . . . . .	29
Do I want/need to include the description of the KDE muon estimation? (YELLOW) . . . . .	29
Blow up labels/legend/title and make it more readable in the margin or move it into the main text? (RED) . . . . .	29
I don't like this formulation, but don't know better right now.. (YELLOW) . . . . .	29
elaborate why this is also done to cover the whole energy range for the pion production, referencing the Barr Block plot that I haven't included yet :D (RED) . . . . .	29
I truly dislike this sentence, too, better ideas? (YELLOW) . . . . .	29
I'm just writing out the data from the table, but I need to mention/motivate the included priors here and maybe just point to the table for the ranges/nominal values? (Not quite sure about this) (RED) . . . . .	29
say something about their priors (RED) . . . . .	30
say something about their priors (RED) . . . . .	30
cite?! (ORANGE) . . . . .	30
I should add some final level effects of some systematics on the 3D binning and maybe discuss how they are different from the signal shape, or so? (ORANGE) . . . . .	30
again, I think fit metric and TS are mixed up a bit (RED) . . . . .	31
Do I want additional plots for this (fit diff, LLH distr, minim. stats, param. fits)? (YELLOW) . . . . .	31
here again, this is just the fit metric, right? (RED) . . . . .	32
Add bin-wise TS distribution? Add 3D TS maps? (RED) . . . . .	32
sort the variables also by type, same as in the table "best_fit_parameters"? (ORANGE) . . . . .	33
Show best fit hole ice angular acceptance compared to nominal and flasher/in-situ fits, maybe? (YELLOW) . . . . .	33
Discuss what it means that the parameters are at these values? Here, or somewhere else? (RED) . . . . .	33
fix table caption (RED) . . . . .	33
fix once I have them produced (RED) . . . . .	34
fix once I have the brazil bands (RED) . . . . .	34
fix caption for this figure (RED) . . . . .	34
make plot with BFPs and limit, comparing to upper limits from other experiments, think about ow to prsent it (RED) . . . . .	34
specify which they are, once I have them (RED) . . . . .	34

add 1-d data/mc agreement for example mass sample (0.6?) and all 3 analysis variables (RED) . . . . .	34
add table with reduced chi2 for all 1-d distributions (RED) . . . . .	34
Re-make plot with x,y for horizontal set one plot! . . . . .	37
Re-make plot with x, y, z for both cascades in one. . . . .	37
Re-arrange plots in a more sensible way. . . . .	37
sort these by type of nuisance parameter? . . . . .	41



# Contents

<b>Abstract</b>	iii
<b>Contents</b>	ix
<b>1 Standard Model Neutrinos and Beyond</b>	<b>1</b>
1.1 The Standard Model . . . . .	1
1.1.1 Fundamental Fields . . . . .	1
1.1.2 Electroweak Symmetry Breaking . . . . .	2
1.1.3 Fermion Masses . . . . .	3
1.1.4 Weak Interactions after Symmetry-Breaking . . . . .	3
1.2 Beyond the Standard Model . . . . .	3
1.2.1 Mass Mechanisms . . . . .	4
1.2.2 Observational Avenues for Right-Handed Neutrinos . . . . .	5
1.2.3 Searching for Heavy Neutral Leptons . . . . .	6
1.3 Atmospheric Neutrinos as Source of Heavy Neutral Leptons . . . . .	6
1.3.1 Production of Neutrinos in the Atmosphere . . . . .	6
1.3.2 Interactions with Nuclei . . . . .	7
1.3.3 Oscillations . . . . .	8
1.3.4 Testing Heavy Neutral Leptons with Atmospheric Neutrinos . . . . .	10
<b>2 Detecting Low Energetic Double Cascades</b>	<b>15</b>
2.1 Reconstruction . . . . .	15
2.1.1 Table-Based Minimum Likelihood Algorithms . . . . .	15
2.1.2 Optimization for Low Energy Events . . . . .	16
2.1.3 Performance . . . . .	18
2.2 Double Cascade Classification . . . . .	21
2.3 Cross Checks . . . . .	21
2.3.1 Simplistic Sets . . . . .	21
2.4 Performance . . . . .	22
2.4.1 Energy/Decay Length Resolution . . . . .	22
2.5 Low Energy Event Selection Efficiency . . . . .	25
<b>3 Search for an Excess of Heavy Neutral Lepton Events</b>	<b>27</b>
3.1 Final Level Sample . . . . .	27
3.1.1 Expected Rates/Events . . . . .	27
3.1.2 Analysis Binning . . . . .	28
3.2 Statistical Analysis . . . . .	28
3.2.1 Low Energy Analysis Framework . . . . .	28
3.2.2 Test Statistic . . . . .	29
3.2.3 Physics Parameters . . . . .	29
3.2.4 Nuisance Parameters . . . . .	29
3.3 Analysis Checks . . . . .	31
3.3.1 Minimization Robustness . . . . .	31
3.3.2 Goodness of Fit . . . . .	31
3.4 Results . . . . .	32
3.4.1 Best Fit Nuisance Parameters . . . . .	32
3.4.2 Best Fit Parameters and Limits . . . . .	33
3.4.3 Data/MC Agreement . . . . .	34

<b>APPENDIX</b>	<b>35</b>
<b>A Heavy Neutral Lepton Signal Simulation</b>	<b>37</b>
A.1 Model Independent Simulation Distributions . . . . .	37
A.2 Model Dependent Simulation Distributions . . . . .	38
<b>B Analysis Checks</b>	<b>39</b>
B.1 Minimization Robustness . . . . .	39
B.2 Ensemble Tests . . . . .	39
<b>C Analysis Results</b>	<b>41</b>
C.1 Best Fit Nuisance Parameters . . . . .	41
C.2 Best Fit Parameters and Limits . . . . .	41
<b>Bibliography</b>	<b>43</b>

# List of Figures

1.1	Feynman diagrams of neutrino weak interactions . . . . .	3
1.2	HNL decay widths . . . . .	6
1.3	Atmospheric neutrino fluxes . . . . .	7
1.4	Neutrino-nucleon deep inelastic scattering . . . . .	8
1.5	Total inclusive neutrino-nucleon cross-sections . . . . .	9
1.6	Current $ U_{\tau 4}^2  - m_4$ limits . . . . .	11
1.7	Feynman diagram of HNL up-scattering process . . . . .	12
1.8	Feynman diagram of HNL decay . . . . .	13
1.9	HNL branching ratios . . . . .	13
2.2	short . . . . .	17
2.3	Preliminary 2-d reconstructed versus true cascade energy resolutions . . . . .	19
2.4	Preliminary 2-d reconstructed versus true decay length resolutions . . . . .	20
3.1	xx . . . . .	29
3.2	Asimov inject/recover test (0.6 GeV) . . . . .	32
3.3	Pseudo-data trials TS distribution (0.6 GeV) . . . . .	32
3.4	Best fit nuisance parameter distances to nominal . . . . .	33
3.5	xx . . . . .	34
A.1	Simplified model independent simulation generation level distributions . . . . .	37
A.2	Realistic model independent simulation generation level distributions . . . . .	38
A.3	Model dependent simulation generation level distributions . . . . .	38
B.1	Asimov inject/recover test (0.3 GeV, 1.0 GeV) . . . . .	39
B.2	Pseudo-data trials TS distribution (0.3 GeV, 1.0 GeV) . . . . .	39
C.1	xx . . . . .	42



# List of Tables

1.1	Standard model fermions . . . . .	2
3.1	Final level background event/rate expectation . . . . .	27
3.2	Final level signal event/rate expectation . . . . .	28
3.3	Analysis binning . . . . .	28
3.4	Nuisance parameter nominal values and fit ranges . . . . .	30
3.5	Staged minimization routine settings . . . . .	31
3.6	xx . . . . .	34
C.1	xx . . . . .	41



# Standard Model Neutrinos and Beyond

1

## 1.1 The Standard Model

The *Standard Model (SM)* of particle physics is a Yang-Mills theory [1] providing very accurate predictions of weak, strong, and *electromagnetic (EM)* interactions. It is a relativistic quantum field theory that relies on gauge invariance, where all matter is made up of fermions, which are divided into quarks and leptons, and bosons describe the interactions between the fermions that have to fulfil the overall symmetry of the theory. Leptons are excitations of Dirac-type fermion fields.

The initial idea of the theory is associated with the works of Weinberg [2], Glashow [3], and Salam [4], that proposed a unified description of EM and weak interactions as a theory of a spontaneously broken  $SU(2) \times U(1)$  symmetry for leptons, predicting a neutral massive vector boson  $Z^0$ , a massive charged vector boson  $W^\pm$ , and a massless photon  $\gamma$  as the gauge bosons. The Higgs mechanism [5], describing the breaking of the symmetry, predicts the existence of an additional scalar particle, the Higgs boson, giving the  $W^\pm$  and  $Z^0$  bosons their mass. The Higgs boson was discovered in 2012 at the LHC.

Gell-Mann and Zweig proposed the quark model in 1964 [6, 7], which was completed by the discovery of non-abelian gauge theories [8] to form the  $SU(3)$  symmetry of the strong interaction called *quantum chromodynamics (QCD)*. QCD describes the interaction between quarks and gluons which completed the full picture of the SM in the mid-1970s. Together with the electroweak theory, the SM is a  $SU(3)_C \times SU(2)_L \times U(1)_Y$  local gauge symmetry, with the conserved quantities  $C$ , *color*,  $L$ , *left-handed chirality*, and  $Y$ , *weak hypercharge*.

In the following, the basic properties of the SM are described, following the derivations of [9, 10].

### 1.1.1 Fundamental Fields

Fermions in the SM are Weyl fields with either *left-handed (LH)* or *right-handed (RH)* chirality, meaning they are eigenvectors of the chirality operator  $\gamma_5$  with  $\gamma_5 \psi_{R/L} = \pm \psi_{R/L}$ . Only LH particles transform under  $SU(2)_L$ . The Higgs field is a complex scalar field, a doublet of  $SU(2)_L$ , which is responsible for the spontaneous symmetry breaking of  $SU(2)_L \times U(1)_Y$  to  $U(1)_{\text{EM}}$ . Local gauge transformations of the fields are given by

$$\psi \rightarrow e^{ig\theta^a(x)T^a} \psi , \quad (1.1)$$

where  $g$  is the coupling constant,  $\theta^a(x)$  are the parameters of the transformation, and  $T^a$  are the generators of the group, with  $a$  counting them. The number of bosons is dependent on the generators of the symmetry groups, while the strength is defined by the coupling constants. There are eight massless gluons corresponding to the generators of the  $SU(3)_C$  group. These

1.1 The Standard Model	1
1.2 Beyond the Standard Model . . . . .	3
1.3 Atmospheric Neutrinos as source of Heavy Neutral Leptons . . . . .	6

[1]: Yang et al. (1954), "Conservation of Isotopic Spin and Isotopic Gauge Invariance"

[2]: Weinberg (1967), "A Model of Leptons"

[3]: Glashow (1961), "Partial-symmetries of weak interactions"

[5]: Higgs (1964), "Broken symmetries, massless particles and gauge fields"

Also cite this? Didn't find a good reference, only the press releases.

[6]: Gell-Mann (1964), "A Schematic Model of Baryons and Mesons"

[7]: Zweig (1964), "An  $SU(3)$  model for strong interaction symmetry and its breaking. Version 2"

[9]: Giunti et al. (2007), *Fundamentals of Neutrino Physics and Astrophysics*

[10]: Schwartz (2013), *Quantum Field Theory and the Standard Model*

mediate the strong force which conserves color charge. The  $W_1, W_2, W_3$ , and  $B$  boson fields of the  $SU(2)_L \times U(1)_Y$  group are mixed into the massive bosons through spontaneous symmetry breaking as

$$W^\pm = \frac{1}{\sqrt{2}}(W_1 \mp iW_2) \quad (1.2)$$

and

$$Z^0 = \cos \theta_W W_3 - \sin \theta_W B, \quad (1.3)$$

with  $\theta_W$  being the *Weinberg angle*. The massless photon field is given by

$$A = \sin \theta_W W_3 + \cos \theta_W B \quad (1.4)$$

and its conserved quantity is the EM charge  $Q$ , which depends on the weak hypercharge,  $Y$ , and the third component of the weak isospin,  $T_3$ , as  $Q = T_3 + Y/2$ .

	Type			$Q$
quarks	u	c	t	+2/3
	d	s	b	-1/3
leptons	$\nu_e$	$\nu_\mu$	$\nu_\tau$	0
	e	$\mu$	$\tau$	-1

**Table 1.1:** Fermions in the Standard Model. Shown are all three generations of quarks and leptons with their electric charge  $Q$ .

Fermions are divided into six quarks and six leptons. Weak, strong, and EM force act on the quarks, and they are always found in bound form as baryons or mesons. Leptons do not participate in the strong interaction and only the electrically charged leptons are massive and are effected by the EM force, while neutrinos are massless and only interact via the weak force. Each charged lepton has an associated neutrino, which it interacts with in *charged-current (CC)* weak interactions, that will be explained in more detail in Section 1.1.4. The fermions are listed in Table 1.1.

### 1.1.2 Electroweak Symmetry Breaking

To elaborate the process of spontaneous symmetry breaking through which the gauge bosons of the weak interaction acquire their masses, the Lagrangian of the Higgs field is considered as

$$\mathcal{L}_{\text{Higgs}} = (D_\mu \Phi^\dagger)(D^\mu \Phi) - \lambda \left( \Phi^\dagger \Phi - \frac{v^2}{2} \right)^2, \quad (1.5)$$

with parameters  $\lambda$  and  $v$ , where  $\lambda$  is assumed to be positive.  $\Phi$  is the Higgs doublet, which is defined as

$$\Phi = \begin{pmatrix} \Phi^+ \\ \Phi^0 \end{pmatrix}, \quad (1.6)$$

with the charged component  $\Phi^+$  and the neutral component  $\Phi^0$ . The covariant derivative is given by

$$D_\mu = \partial_\mu - ig_2 \frac{\sigma^i}{2} W_\mu^i - \frac{1}{2}ig_1 B_\mu, \quad (1.7)$$

with the Pauli matrices  $\sigma^i$  and the gauge boson fields  $W_\mu^i$  and  $B_\mu$  of the  $SU(2)_L$  and  $U(1)_Y$  groups, respectively. The coupling constants  $g_2$  and  $g_1$  are the respective coupling constants which are related to the Weinberg angle as  $\tan \theta_W = \frac{g_1}{g_2}$ . The Higgs potential has a non-zero *vacuum expectation value (vev)* at the minimum of the potential at  $\Phi^\dagger \Phi = \frac{v^2}{2}$ . Since the vacuum is electrically neutral, it can only come from a neutral component of the Higgs

doublet as

$$\Phi_{\text{vev}} = \frac{1}{\sqrt{2}} \begin{pmatrix} 0 \\ v \end{pmatrix}. \quad (1.8)$$

### 1.1.3 Fermion Masses

The mass term for charged fermions with spin-1/2 is given by

$$\mathcal{L}_{\text{Dirac}} = m(\bar{\Psi}_R \Psi_L - \bar{\Psi}_L \Psi_R), \quad (1.9)$$

composed of the product of left- and RH Weyl spinors  $\Psi_{L/R}$ . This term is not invariant under  $SU(2)_L \times U(1)_Y$  gauge transformations, but adding a Yukawa term

$$\mathcal{L}_{\text{Yukawa}} = -y \bar{L}_L \Phi e_R + h.c., \quad (1.10)$$

coupling the fermion fields to the Higgs field, recovers the invariance and gives the fermions their masses. Here,  $y$  is the Yukawa coupling constant and  $\bar{L}_L$  is the  $SU(2)_L$  doublet. With the vev, this results in the mass term for the charged leptons and down-type quarks of  $-m_e(\bar{e}_L e_R + \bar{e}_R e_L)$  with  $m_e = \frac{yv}{\sqrt{2}}$ . With  $\tilde{\Phi} = i\sigma_2 \Phi^*$ , a similar Yukawa term can be written as  $-y \bar{L}_L \tilde{\Phi} u_R + h.c.$ , which leads to the masses of the up-type quarks.

### 1.1.4 Weak Interactions after Symmetry-Breaking

#### Stuff from my MSc thesis to re-write:

In the SM, weak interactions are mediated by the three massive bosons  $W^+$ ,  $W^-$ , and  $Z^0$  [12]. The large boson masses ( $m_W \sim 80 \text{ GeV}$ ,  $m_Z \sim 90 \text{ GeV}$ ) result in a short range of the force of about  $10 \times 10^{-18} \text{ m}$ . Weak interactions carried by  $W^\pm$  bosons are called CC interactions, because charge is transferred between the interacting particles. In CC interactions, a neutrino is converted into its corresponding charged lepton or vice versa. Neutral current (NC) interactions are those mediated by  $Z^0$  bosons. Here no charge is transferred. The Feynman diagrams for CC and NC interactions are shown in Figure 1.1.

The observed phenomenon of neutrino oscillations (see Section 1.3.3) is based on the fact that there is a mass difference between the three neutrino mass eigenstates.

Introduce SM EW NC/CC Lagrangian to build upon in the next chapter

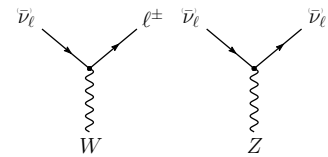


**Figure 1.1:** Feynman diagrams of charged-current (left) and neutral-current (right) neutrino weak interactions, taken from [11].

Plot is missing + for W and 0 for Z boson.

[12]: Thomson (2013), *Modern particle physics*

## 1.2 Beyond the Standard Model

#### Open questions related to neutrinos:

- ▶ question of neutrino nature, e.g. dirac or majorana?
- ▶ absolute mass values? (mass ordering + absolute mass scale)
- ▶ is there leptonic cp violation and what is the precise delta\_cp value?
- ▶ what are the mixing angle values and is there a flavor principle
- ▶ is there additional effects like steriles, non-standard, lorentz violation

Are the fundamentals of the SM described above enough to explain *all* observed phenomena? Gravity cannot be explained by the SM, as it is incompatible with general relativity. Neither can the SM explain some cosmological observations like dark matter, and the matter-antimatter asymmetry, and it does not predict neutrinos to have mass, which is experimentally proven by neutrino oscillations, so some extensions to the SM is needed in order to explain them.

Cite and/or sidenote this.

Standard cosmology ( $\Lambda$ CDM) assumes that equal amounts of matter and anti-matter were produced in the early universe. However, the universe today is dominantly made up of matter. This so-called *baryon asymmetry* can be measured by the difference between the number densities of baryons and anti-baryons normalized to the number density of photons as

$$\eta_B = \frac{n_B - n_{\bar{B}}}{n_\gamma} , \quad (1.11)$$

cite this

where  $n_B$ ,  $n_{\bar{B}}$ , and  $n_\gamma$  are the number densities of baryons, anti-baryons, and photons, respectively. Baryons are the dominant component with  $\eta_B$  being observed to be around  $6 \times 10^{-10}$ . Leptogenesis and EW baryogenesis are scenarios that could explain this phenomenon, where the former could be realized by the existence of heavy RH neutrinos.

- [13]: Davis et al. (1968), "Search for Neutrinos from the Sun"
- [14]: Fukuda et al. (1998), "Evidence for Oscillation of Atmospheric Neutrinos"
- [15]: Ahmad et al. (2002), "Direct Evidence for Neutrino Flavor Transformation from Neutral-Current Interactions in the Sudbury Neutrino Observatory"

cite neutrino oscillations/flavor conversions

The observation of neutrino flavor conversions and neutrino oscillations in a multitude of experiments[13–15] is the strongest evidence for physics beyond the SM measured in laboratories. The observation that neutrinos change their flavor while they propagate through space can only be explained, if at least two neutrinos have a non-zero mass. From the measurements and cosmological observations, we know that the masses are very small as compared to the lepton masses. Neither their existence, nor their smallness is not predicted by the SM, but adding additional RH neutrinos states to the theory could explain the origin of the observed non-zero neutrino masses and could be tested for by searching for corresponding signatures in experiments. But the addition of RH neutrino fields is not the only possible explanation for neutrino masses. Radiative neutrino mass mechanisms could also explain their origin and their smallness, but those would need the introduction of additional symmetries to the theory.

- [16]: Tanabashi et al. (2018), "Review of Particle Physics"
- [17]: Aker et al. (2022), "Direct neutrino-mass measurement with sub-electronvolt sensitivity"
- [18]: Alam et al. (2021), "Completed SDSS-IV extended Baryon Oscillation Spectroscopic Survey: Cosmological implications from two decades of spectroscopic surveys at the Apache Point Observatory"
- [19]: Aghanim et al. (2020), "Planck2018 results: VI. Cosmological parameters"

namedrop  
RH=sterile=HNL and  
why they are called like  
this based on the SM EW  
Lagrangian introduced  
above

Maybe also add this somehow: "From neutrino oscillation measurements the absolute mass scale cannot be determined, since they only depend on the mass differences, but there are upper limits on the sum of all neutrino masses from cosmological observations. These upper limits are typically between 0.3 and 1.3 eV [16]." "Actually 0.8 eV [17] from KATRIN and 1.2 eV [18, 19] from cosmological observations."

### 1.2.1 Mass Mechanisms

There are no RH neutrinos in the SM and therefore the mass mechanism described in Section 1.1.3, which couples the Higgs field to LH and RH Weyl fields, predicts them to be massless. From experimental observations it is known that at least two of the three neutrino generations need to have a non-zero mass. Assuming the existence of RH neutrinos fields  $\nu_R$ , one way of producing the neutrino masses is by adding a Yukawa coupling term

similar to the one for up-type quarks mentioned in Section 1.1.3, to write the full Yukawa Lagrangian as

$$\mathcal{L}_{\text{Yukawa}} = -Y_{ij}^e \tilde{L}_L^i \Phi e_R^j - Y_{ij}^\nu \tilde{L}_L^i \tilde{\Phi} \nu_R^j + h.c. , \quad (1.12)$$

with  $i, j$  running over the three generations of leptons  $e, \mu$ , and  $\tau$ , and  $Y^e$  and  $Y^\nu$  being the Yukawa coupling matrices. Diagonalizing the Yukawa coupling matrices through unitary transformations  $U^e$  and  $U^\nu$  leads to the **Dirac mass term** in the mass basis as

$$\mathcal{L}_{\text{Dirac}}^{\text{mass}} = \frac{v}{\sqrt{2}} (\bar{e}_L M_e e_R - \bar{\nu}_L M_\nu \nu_R) , \quad (1.13)$$

where  $M_e$  and  $M_\nu$  are the diagonal mass matrices of leptons and neutrinos, respectively. A purely Dirac mass term would not explain the smallness of the neutrino masses in a straightforward way. Only fine-tuning the Yukawa coupling constants to small values would lead to small neutrino masses.

An additional way of generating neutrino masses is by adding a Majorana mass term of the form

$$\mathcal{L}_{\text{Majorana}} = -\frac{1}{2} M_{ij} (\nu_R^i)^c \nu_R^j + h.c. , \quad (1.14)$$

with  $M_{ij}$  being the Majorana mass matrix and the indices  $i, j$  running over all  $N_R$  RH neutrino generations. The superscript  $c$  denotes the charge conjugate field. Combining the charge conjugated RH neutrino fields with the LH neutrino fields as

$$N = \begin{pmatrix} \nu_L \\ \nu_R^c \end{pmatrix} , \quad (1.15)$$

with  $\nu_R$  containing the  $N_R$  RH fields. The full neutrino mass Lagrangian is then given by the combined **Dirac and Majorana mass term** as

$$\mathcal{L}_{\text{Dirac+Majorana}}^{\text{mass},\nu} = \frac{1}{2} N^T \hat{C} M^{D+M} N + h.c. , \quad (1.16)$$

and the mass matrix is given by

$$M^{D+M} = \begin{pmatrix} 0 & (M^D)^T \\ M^D & M^R \end{pmatrix} . \quad (1.17)$$

On top of explaining the origin of neutrino masses itself, a combined Dirac and Majorana mass term could also solve the question of their smallness. If the mass of the RH neutrinos is very large, the masses of the active neutrino flavors is suppressed, which is known as *see-saw mechanism*.

## 1.2.2 Observational Avenues for Right-Handed Neutrinos

- ▶ oscillations searches for light steriles
- ▶ potential searches for heavy steriles

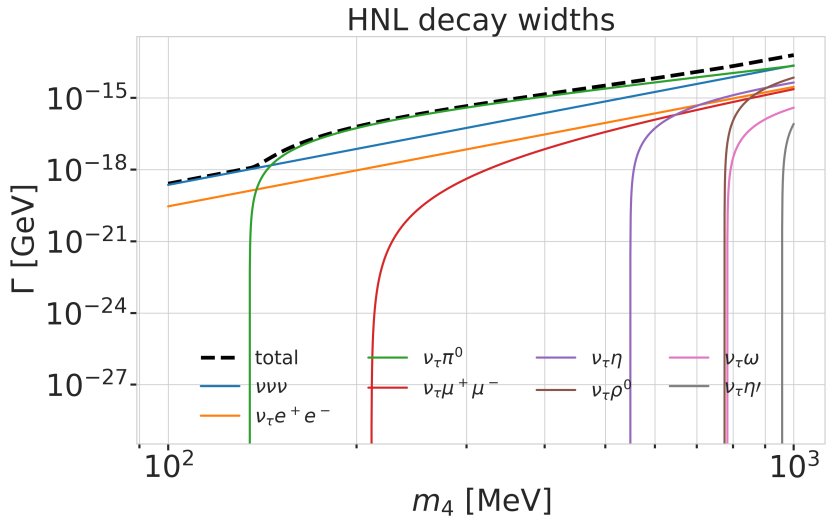


**Figure 1.2:** Decay widths of the HNL within the mass range considered, calculated based on the results from [20]. Given the existing constraints on  $|U_{e4}|^2$  and  $|U_{\mu 4}|^2$ , we consider that the corresponding decay modes are negligible.

### 1.2.3 Searching for Heavy Neutral Leptons

Collider

Nuclear Decay

Extracted Beamlines

Atmospheric and Solar

Cosmological and Astrophysical

## 1.3 Atmospheric Neutrinos as Source of Heavy Neutral Leptons

write some interlude to motivate atm. neutrinos as source for HNL searches/production etc.

### 1.3.1 Production of Neutrinos in the Atmosphere

The analysis performed in this work is based on the sample of neutrinos observed in IceCube DeepCore at energies below 100 GeV. At these energies, the flux exclusively originates in the Earth's atmosphere. Highly relativistic cosmic rays (protons and heavier nuclei [16]) interact in the upper atmosphere, producing showers of secondary particles. Neutrinos are produced in decays of charged pions and kaons ( $\pi$  and  $K$  mesons) present in those showers, where the dominant contribution comes from the decay chain

$$\begin{aligned} \pi^\pm &\rightarrow \mu^\pm + \nu_\mu (\bar{\nu}_\mu), \\ \mu^\pm &\rightarrow e^\pm + \bar{\nu}_\mu (\nu_\mu) + \nu_e (\bar{\nu}_e), \end{aligned} \quad (1.18)$$

where muon neutrinos  $\nu_\mu$  and muons  $\mu^\pm$  are produced in the first decay and both electron and muon neutrinos  $\nu_{e/\mu}$  are produced in the second decay. Atmospheric muons, which are also produced in these decays, are the main background component for IceCube DeepCore analyses.

[16]: Tanabashi et al. (2018), "Review of Particle Physics"

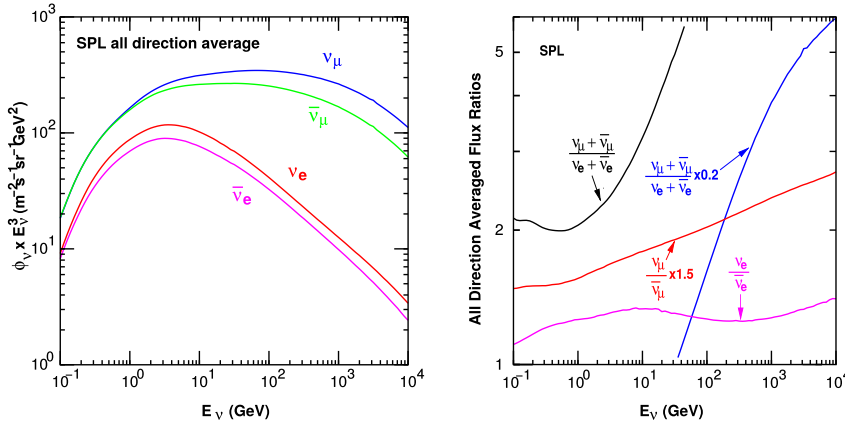


**Figure 1.3:** The atmospheric fluxes of different neutrino flavors as a function of energy (left) and the ratios between muon neutrinos and electron neutrinos as well as the ratios between neutrinos and antineutrinos for both those flavors (right). Results from the calculations performed for the geographic South Pole, taken from [21].

The different atmospheric flux components are shown in Figure 1.3 (left), for a much broader energy range than relevant for this work. Both neutrinos and antineutrino fluxes are shown for electron and muon neutrinos and all fluxes are the directionally averaged expectation calculated at the South Pole. Muon neutrinos are dominating the flux and from Equation 1.18 the naive assumption would be that the ratio between muon and electron neutrinos is  $(\nu_\mu + \bar{\nu}_\mu)/(\nu_e + \bar{\nu}_e) = 2$ . This is roughly true at energies below 1 GeV, where all muons decay in flight, but at larger energies muons can reach the detector before decaying, which increases the ratio to approximately 10:1 at around 100 GeV. Additionally, kaon decays start to contribute which also increases the number of muons and muon neutrinos. The increasing ratio can be seen in Figure 1.3 (right), which also shows the ratio between neutrinos and antineutrinos for both flavors.

Charged mesons or tau particles can also be produced in cosmic ray interactions. Their decays lead to the production of tau neutrinos. At the energies relevant for this work however, the resulting tau neutrino flux is negligible as compared to the muon neutrino flux [22] and is not considered in the analysis. This is because both charged mesons and tau particles are much heavier than pions and kaons and therefore their production is suppressed at high energies.

[22]: Fedynitch et al. (2015), “Calculation of conventional and prompt lepton fluxes at very high energy”

Say something about atmospheric neutrino flux uncertainties, based on recent JP/Anatoli papers.

### 1.3.2 Interactions with Nuclei

The neutrino detection principle of IceCube DeepCore is explained in Chapter ?? and relies on the weak interaction processes between neutrinos and the nuclei of the Antarctic glacial ice. At neutrino energies above 5 GeV, the cross-sections are dominated by *deep inelastic scattering (DIS)*, where the neutrino is energetic enough to resolve the underlying structure of the nucleons and interact with one of the composing quarks individually. As a result the nucleon breaks and a shower of hadronic secondary particles is produced. Depending on the type of interaction, the neutrino either remains in the final state for NC interactions or is converted into its charged lepton counterpart for CC interactions. The CC DIS interactions have the form

$$\begin{aligned} \nu_l + N &\rightarrow l^- + X , \\ \bar{\nu}_l + N &\rightarrow l^+ + X , \end{aligned} \quad (1.19)$$

where  $\nu_l/\bar{\nu}_l$  and  $l^-/l^+$  are the neutrino/antineutrino and its corresponding lepton/antilepton, and  $l$  can be either an electron, muon, or tau.  $N$  is the nucleon and  $X$  stands for any set of final state hadrons. The NC DIS interactions are

$$\begin{aligned} \nu_l + N &\rightarrow \nu_l + X \text{ and} \\ \bar{\nu}_l + N &\rightarrow \bar{\nu}_l + X . \end{aligned} \quad (1.20)$$

Figure 1.4 shows the Feynman diagrams for both processes DIS interactions

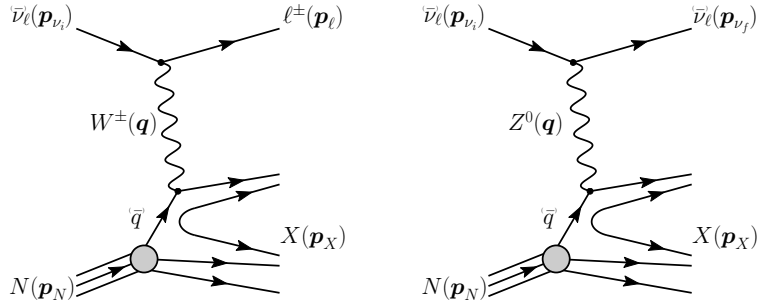


**Figure 1.4:** Feynman diagrams for deep inelastic scattering of a neutrino with a nucleon via charged-current (left) and neutral current (right) interactions.  $p_{\nu_i}, p_N$  and  $p_{\nu_f}$ ,  $p_l, p_N$  are the input and output four-momenta, while  $q$  is the momentum transfer. Taken from [11].

have a roughly linear energy dependent cross-section above  $\sim 20$  GeV and are well measured and easy to theoretically calculate. They are the primary interaction channel for neutrinos detected with IceCube.

At energies below 5 GeV, **quasi-elastic scattering (QE)** and **resonant scattering (RES)** become important. At these energies the neutrinos interact with the approximately point-like nucleons, without breaking them up in the process. RES describes the process of a neutrino scattering off a nucleon producing an excited state of the nucleon in addition to a charged lepton. It is the dominant process at 1.5 GeV to 5 GeV for neutrinos and 1.5 GeV to 8 GeV for antineutrinos. Below 1.5 GeV QE is the main process, where protons are converted to neutrons in antineutrino interactions and vice-versa for neutrino interactions. Additionally, a charged lepton corresponding to the neutrino/antineutrino flavor is produced. The cross-sections of QE and RES scattering processes are not linear in energy and the transition region from QE/RES to DIS is poorly understood. The total cross-sections and their composition is shown in Figure 1.5. It can be seen that the interaction cross-sections are very small at the order of  $10^{-38}$  cm $^2$ . This is the reason why very large volume detectors are required to measure atmospheric neutrinos with sufficient statistics to perform precision measurements of their properties. The interaction length of a neutrino with  $E_\nu = 10$  GeV is of  $\mathcal{O}(10 \times 10^{10}$  km), for example.

### 1.3.3 Oscillations

So far we have described neutrinos in their flavor eigenstates, which are relevant for weak interactions. In the SM three-neutrino model the weak flavor states are  $\nu_e, \nu_\mu$ , and  $\nu_\tau$ , which relate them to the charged leptons they interact with in CC interactions. There is a second way of describing neutrino wave functions based on their Hamiltonian eigenvalues [24], namely as the mass eigenstates  $\nu_1, \nu_2$ , and  $\nu_3$ . These states are related to the flavor eigenstates by the unitary, 3x3 Pontecorvo-Maki-Nakagawa-Sakata (PMNS)

[24]: Bilenky et al. (1978), “Lepton mixing and neutrino oscillations”

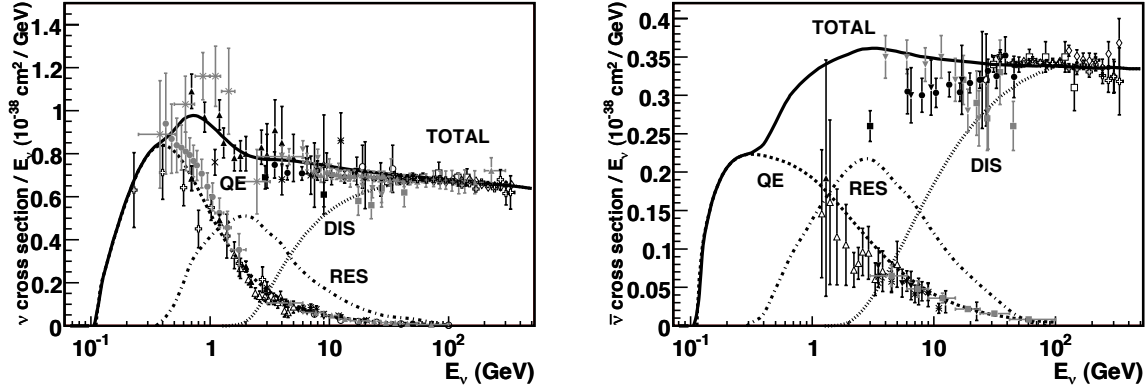


**Figure 1.5:** Total neutrino (left) and antineutrino (right) per nucleon cross-section divided by neutrino energy plotted against energy. The three main scattering processes quasi-elastic scattering (QE), resonant scattering (RES), and deep-inelastic scattering (DIS) are shown. Taken from [23].

matrix  $U$ , where the flavor states are a superposition of the mass states as

$$|\nu_\alpha\rangle = \sum_k U_{ak}^* |\nu_k\rangle , \quad (1.21)$$

with the weak flavor states  $|\nu_\alpha\rangle$ ,  $\alpha = e, \mu, \tau$ , and the mass states  $|\nu_k\rangle$  with  $k = 1, 2, 3$ . The mixing matrix can be parameterized as [16]

$$U = \begin{pmatrix} 1 & 0 & 0 \\ 0 & c_{23} & s_{23} \\ 0 & -s_{23} & c_{23} \end{pmatrix} \begin{pmatrix} c_{13} & 0 & s_{13}e^{-i\delta_{CP}} \\ 0 & 1 & 0 \\ -s_{13}e^{i\delta_{CP}} & 0 & c_{13} \end{pmatrix} \begin{pmatrix} c_{12} & s_{12} & 0 \\ -s_{12} & c_{12} & 0 \\ 0 & 0 & 1 \end{pmatrix}, \quad (1.22)$$

[16]: Tanabashi et al. (2018), "Review of Particle Physics"

where  $c_{ij} = \cos \theta_{ij}$  and  $s_{ij} = \sin \theta_{ij}$  are cosine and sine of the mixing angle  $\theta_{ij}$ , that defines the strength of the mixing between the mass eigenstates  $i$  and  $j$ , and  $\delta_{CP}$  is the neutrino CP-violating phase.

Describing neutrinos in their mass state is crucial to understand their propagation through space and time. Their propagation in vacuum can be expressed by applying a plane wave approach, where the mass eigenstates evolve as

$$|\nu_k(t)\rangle = e^{-iE_k t/\hbar} |\nu_k\rangle . \quad (1.23)$$

add current BF values  
from nufit or so?

The energy of the mass eigenstate  $|\nu_k\rangle$  is  $E_k = \sqrt{\vec{p}^2 c^2 + m_k^2 c^4}$ , with momentum  $\vec{p}$  and mass  $m_k$ ,  $\hbar$  is the reduced Planck constant, and  $c$  is the speed of light in vacuum. The existence of non-zero, non-equal masses and the neutrino mixing relation in Equation 1.21, lead to the observed phenomenon of neutrino oscillations. Oscillations mean that a neutrino changes from its initial flavor, that it was produced with, to another flavor and back after traveling a certain distance. A neutrino is produced as a flavor eigenstate  $|\nu_\alpha\rangle$  in a CC weak interaction, but its propagation happens as the individual mass states it is composed of. The probability of finding the neutrino with initial flavor  $|\nu_\alpha\rangle$  in the flavor state  $|\nu_\beta\rangle$  after the time  $t$  is calculated as

$$P_{\nu_\alpha \rightarrow \nu_\beta}(t) = |\langle \nu_\beta | \nu_\alpha(t) | \nu_\beta | \nu_\alpha(t) \rangle|^2 , \quad (1.24)$$

by applying Fermi's Golden Rule [25], which defines the transition rate from one eigenstate to another by the strength of the coupling between them. This coupling strength is the square of the matrix element and using the fact that the mixing matrix is unitary ( $U^{-1} = U^\dagger$ ) to describe the mass eigenstates

[25]: Dirac (1927), "The Quantum Theory of the Emission and Absorption of Radiation"

as flavor eigenstates, we find the time evolution of the flavor state  $|\nu_\alpha(t)\rangle$ , which can be inserted into Equation 1.24 to find the probability as

$$P_{\nu_\alpha \rightarrow \nu_\beta}(t) = \sum_{j,k} U_{\beta j}^* U_{\alpha j} U_{\beta k} U_{\alpha k}^* e^{-i(E_k - E_j)t/\hbar}. \quad (1.25)$$

The indices  $j$  and  $k$  run over the mass eigenstates. We can approximate the energy as

$$E_k \approx E + \frac{c^4 m_k^2}{2E} \longrightarrow E_k - E_j \approx \frac{c^4 \Delta m_{kj}^2}{2E}, \quad (1.26)$$

for small neutrino masses compared to their kinetic energy. Here,  $\Delta m_{kj}^2 = m_k^2 - m_j^2$  is the mass-squared splitting between states  $k$  and  $j$ . Replacing the time in Equation 1.25 by the distance traveled by relativistic neutrinos  $t \approx L/c$  we get

$$\begin{aligned} P_{\nu_\alpha \rightarrow \nu_\beta}(t) &= \delta_{\alpha\beta} - 4 \sum_{j>k} \text{Re}(U_{\beta j}^* U_{\alpha j} U_{\beta k} U_{\alpha k}^*) \sin^2\left(\frac{c^3 \Delta m_{kj}^2}{4E\hbar} L\right) \\ &\quad + 2 \sum_{j>k} \text{Im}(U_{\beta j}^* U_{\alpha j} U_{\beta k} U_{\alpha k}^*) \sin^2\left(\frac{c^3 \Delta m_{kj}^2}{4E\hbar} L\right), \end{aligned} \quad (1.27)$$

which is called the survival probability if  $\alpha = \beta$ , and the transition probability if  $\alpha \neq \beta$ . Once again, this probability is only non-zero if there are neutrino mass eigenstates with masses greater than zero. Additionally, there must be a mass-squared difference  $\Delta m^2$  and non-zero mixing between the states. Since we assumed propagation in vacuum in Equation 1.23, the transition and survival probabilities correspond to vacuum mixing.

say something about how this changes with matter

### 1.3.4 Testing Heavy Neutral Leptons with Atmospheric Neutrinos

Re-write/re-formulate this section (copied from HNL technote).

[26]: Yanagida (1980), "Horizontal Symmetry and Masses of Neutrinos"

Produce similar styled plot for these limits

[32]: Coloma et al. (2017), "Double-Cascade Events from New Physics in Icecube"

#### The Minimal Standard Model Extension

Extensions to the Standard Model (SM) that add *Heavy Neutral Leptons* (HNLs) provide a good explanation for the origin of neutrino masses through different seesaw mechanisms [26]. While the mixing with  $\nu_e/\mu$  is strongly constrained ( $|U_{\alpha 4}^2| \lesssim 10^{-5} - 10^{-8}$ ,  $\alpha = e, \mu$ ), the mixing with  $\nu_\tau$  is much harder to probe due to the difficulty of producing and detecting  $\nu_\tau$ . Figure 1.6 shows the current limits on the  $\tau$ -sterile mixing space for HNL masses between 0.1 GeV-10 GeV. As was first pointed out in [32], the atmospheric neutrino flux observed in IceCube offers a way to constrain the neutrino-HNL mixing parameters. By using the large fraction of atmospheric  $\nu_\mu$  events that oscillate into  $\nu_\tau$  before they reach the detector, the less constrained  $\tau$ -sterile mixing space can be explored. In this document, we present the methodology and strategy of a search for HNLs with IceCube DeepCore. These additional RH neutrinos can be included in the Standard Model (SM) by extending the PMNS matrix to at least a 3x4 matrix as

$$\begin{pmatrix} \nu_e \\ \nu_\mu \\ \nu_\tau \\ \nu_s \end{pmatrix} = \begin{pmatrix} U_{e1} & U_{e2} & U_{e3} & U_{e4} \\ U_{\mu 1} & U_{\mu 2} & U_{\mu 3} & U_{\mu 4} \\ U_{\tau 1} & U_{\tau 2} & U_{\tau 3} & U_{\tau 4} \\ U_{s1} & U_{s2} & U_{s3} & U_{s4} \end{pmatrix} \begin{pmatrix} \nu_1 \\ \nu_2 \\ \nu_3 \\ \nu_4 \end{pmatrix}, \quad (1.28)$$

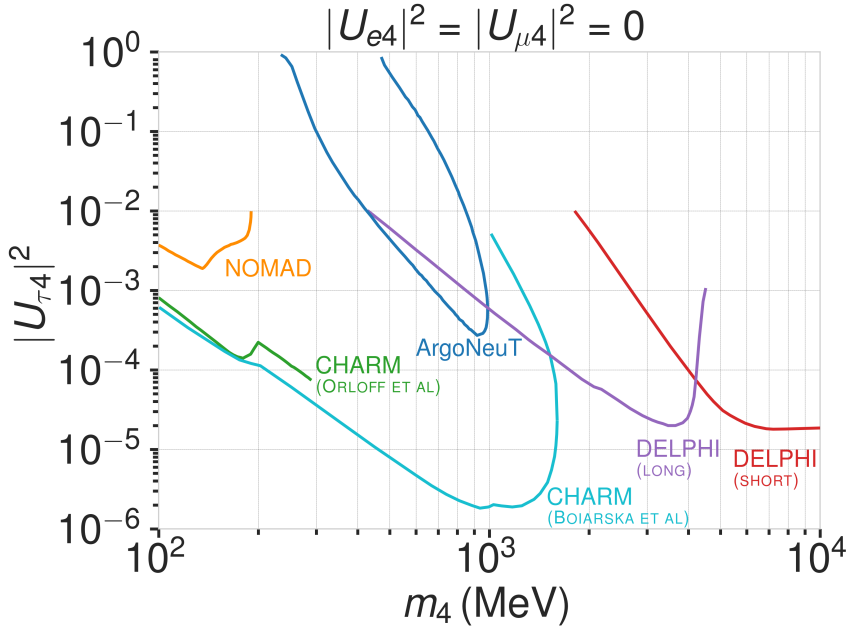


**Figure 1.6:** Current  $|U_{\tau 4}^2| - m_4$  limits from NOMAD [27], ArgoNeut [28], CHARM [29, 30], and DELPHI [31].

where the components with index 4 define the mixing between the flavor states and the fourth sterile mass state, respectively. Note here that this is not a theoretically fully consistent picture, but rather the phenomenologically minimal model to be tested by this analysis. This can hopefully be put into the larger context of several fully consistent models, later. Due to the singlet nature of the RH neutrinos, they only interact weakly, inheriting these interactions from their LH neutrino counterparts via mixing. This mixing of the HNLs with the electron, muon, and tau neutrinos can be probed and constrained as a function of the HNL mass by searching for their production and decay. In [32, 33] this search is mainly motivated through two experimental arguments. Secondly, IceCube is ideally placed to explore the yet unconstrained  $|U_{\tau 4}|^2 - m_4$  phase-space that is not easily accessible by accelerator-based experiments.

In order to probe the  $\tau$ -sterile mixing parameter, it is required to look at interactions involving  $\tau$  neutrinos. However, most neutrinos produced in cosmic ray interactions with the atmosphere are  $\nu_e$  or  $\nu_\mu$ . Therefore, we need these neutrinos to oscillate to the  $\tau$  flavor before reaching the detector. For this to happen at the considered energies a traveled distance of the order of the earth diameter is necessary. This is why our signal is mostly up-going and passing through the whole earth.

[32]: Coloma et al. (2017), “Double-Cascade Events from New Physics in Icecube”

[33]: Coloma (2019), “Icecube/Deep-Core tests for novel explanations of the MiniBooNE anomaly”

This section really needs to be re-written to motivate the search for HNLs from a more generic point of view (e.g. to explain neutrino masses)

This section definitely needs to be elaborated in a little more detail

[20]: Coloma et al. (2021), “GeV-scale neutrinos: interactions with mesons and DUNE sensitivity”

To explain the signature we can observe in IceCube we first have to revisit the weak interactions that the HNL inherits from its LH counterpart through mixing. We will be following the derivation in [20]. Extending the SM by  $n$  additional RH neutrinos,  $\nu_i$  ( $i = 3 + n$ ), leads to the mass Lagrangian

$$\mathcal{L}_v^{\text{mass}} \supset - \sum_{\alpha=e,\mu,\tau} \sum_{i=4}^{3+n} Y_{\nu,\alpha i} \bar{L}_{L,\alpha} \tilde{\phi} \nu_i - \frac{1}{2} \sum_{i=4}^{3+n} M_i \bar{\nu}_i \nu_i^c + h.c., \quad (1.29)$$

in a basis where the Majorana mass terms are diagonal.  $Y_{\nu,\alpha i}$  are the Yukawa couplings to the lepton doublets and  $M$  the Majorana masses for the heavy singlets.  $L_{L,\alpha}$  stands for the SM LH lepton doublet of flavor  $\alpha$  while  $\tilde{\phi}$  is the Higgs field, and  $\tilde{\phi} = i\sigma_2\phi^*$  and  $\nu_i^c \equiv C\bar{\nu}_i^t$ , with  $C = i\gamma_0\gamma_2$  in the

Not adding information about the case where the neutrinos have Dirac or pseudo-Dirac masses

Weyl representation. The full neutrino mass matrix with the Higgs vacuum expectation value  $v/\sqrt{2}$  reads

$$\mathcal{M} = \begin{pmatrix} 0_{3 \times 3} & Y_\nu v/\sqrt{2} \\ Y_\nu^t v/\sqrt{2} & M \end{pmatrix}, \quad (1.30)$$

and can be diagonalized by a  $(3+n) \times (3+n)$  full unitary rotation  $U$ , that itself leads to neutrino masses upon diagonalization, additionally manifesting the mixing between active neutrinos and heavy states. The resulting model consists of 3 light SM neutrino mass eigenstates  $\nu_i$  ( $i = 1, 2, 3$ ) and  $n$  heavier states, as introduced above. The flavor states will now consist of a combination of light and heavy states

$$\nu_\alpha = \sum_{i=1}^{3+n} U_{\alpha i} \nu_i, \quad (1.31)$$

and the leptonic part of the EW Lagrangian can be written as

$$\begin{aligned} \mathcal{L}_{EW}^\ell = & \frac{g}{\sqrt{2}} W_\mu^+ \sum_\alpha \sum_i U_{\alpha i}^* \bar{\nu}_i \gamma^\mu P_L \ell_\alpha + \frac{g}{4c_w} Z_\mu \\ & \times \left\{ \sum_{i,j} C_{ij} \bar{\nu}_i \gamma^\mu P_L \nu_j + \sum_\alpha \bar{\ell}_\alpha \gamma^\mu [2s_w^2 P_R - (1-2s_w^2) P_L] \ell_\alpha \right\} + h.c., \end{aligned}$$

where  $c_w \equiv \cos \theta_w$ ,  $s_w \equiv \sin \theta_w$ , and  $\theta_w$  the SM weak mixing angle or Weinberg angle.  $P_L$  and  $P_R$  are the left and right projectors, respectively, while

$$C_{ij} \equiv \sum_\alpha U_{\alpha i}^* U_{\alpha j}. \quad (1.32)$$

The indices now sum over all  $(3+n)$  flavor and mass states.

Based on this formulation and assuming that only the mixing with the tau sector is open ( $|U_{\alpha 4}^2| = 0$ ,  $\alpha = e, \mu$ ), the relevant production diagram of the HNL can be drawn as shown in Figure 1.7. Alongside the fourth heavy mass state, a Hadronic cascade is produced. The heavy mass state will travel for some distance (dependent on mass and mixing) before it decays. The subsequent decay processes are depicted in Figure 1.8. It can be a CC or NC decay and both leptonic and mesonic modes are possible (dependent on the mass). This will produce a tau or a tau neutrino and another cascade that can be EM or Hadronic. The branching ratios corresponding to the decay modes of the HNL for the mass range of interest (i.e. between 100 MeV and 1 GeV) are shown in Figure 1.9a as a function of the HNL mass.

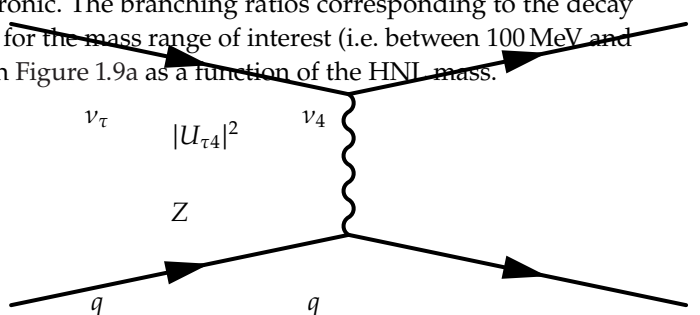


**Figure 1.7:** Production of a sterile neutrino in the up-scattering of a tau neutrino.

### Production and Decay in IceCube DeepCore

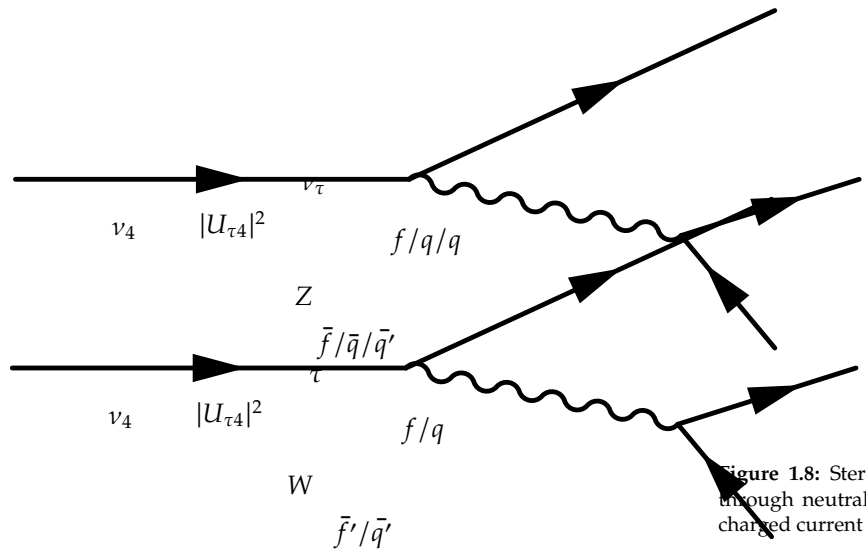


**Figure 1.8:** Sterile neutrino decay through neutral current (left) and charged current (right).

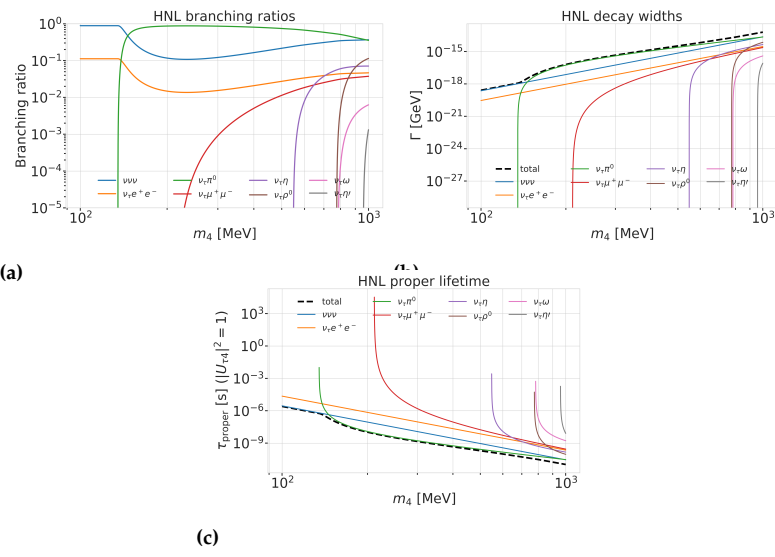


**Figure 1.9:** Branching ratios, decay widths, and proper lifetime of the HNL within the mass range considered, calculated based on the results from [20].



# Detecting Low Energetic Double Cascades

# 2

## 2.1 Reconstruction

All existing reconstruction algorithms applied for low energetic atmospheric neutrino events mentioned in Section ?? are either assuming a single cascade hypothesis or a track and cascade hypothesis, which are the two SM morphologies observable at these energies, as was described in Section ???. A HNL being produced and decaying inside the IceCube detector however, will produce two cascade like light depositions. The morphology and how the cascade properties and their spatial separation depend on the model parameters was introduced in Section 1.3.4. To investigate the performance of the detector to observe these events, a low energetic double cascade reconstruction algorithm was developed, based on a pre-existing algorithm used to search for double cascades produced from high energetic astrophysical tau neutrinos [34] that was established in [35], but first mentioned in [36].

### 2.1.1 Table-Based Minimum Likelihood Algorithms

The reconstruction is relying on a maximum likelihood algorithm, which is the *classical* approach to IceCube event reconstructions, as opposed to ML based methods. A Poissonian likelihood is constructed, which compares the observed photon numbers,  $n$ , with their arrival times to the expected light depositions,  $\mu$ , for a given even hypothesis as

$$\ln(L) = \sum_j \sum_t n_{j,t} \cdot \ln(\mu_{j,t}(\Theta) + \rho_{j,t}) - (\mu_{j,t}(\Theta) + \rho_{j,t}) - \ln(n_{j,t}!) , \quad (2.1)$$

where  $\rho$  are the number of expected photons from noise,  $\Theta$  are the parameters governing the source hypothesis, and the likelihood is calculated summing over all DOMs  $j$  splitting observed photons into time bins  $t$ . The light expectations are calculated using look-up tables [37] that contain the results from MC simulations of reference cascade events or track segments. By varying the parameters defining the event hypothesis, the likelihood of describing the observed light pattern by the expected light depositions is maximized to find the reconstructed event. Algorithms of this kind used in IceCube are described in great detail in [38]. For the table production a specific choice of ice model has to be made, while the calibrated DOM information is taken from the measurement itself.

Based on the tabulated light expectations for cascades and track segments, various event hypothesis can be constructed, like the common cascade only or the track and cascade hypotheses. The hypothesis describing the double cascade signature of the HNL is using two reference cascades that are separated by a certain distance. The whole hypothesis is defined by 9 parameters and assumes that the two cascades are aligned with each other, which is a safe assumption for strongly forward boosted interactions. The parameters are the position of the first cascade  $x, y, z$ , the direction of both cascades  $\phi, \theta$ , and its time  $t$  as well as the decay length  $L$  between the

2.1	Reconstruction	15
2.2	Double Cascade Classification	21
2.3	Cross Checks	21
2.4	Performance	22
2.5	Low Energy Event Selection Efficiency	25

[34]: Abbasi et al. (2020), "Measurement of Astrophysical Tau Neutrinos in IceCube's High-Energy Starting Events"

[35]: Usner (2018), "Search for Astrophysical Tau-Neutrinos in Six Years of High-Energy Starting Events in the IceCube Detector"

[36]: Hallen (2013), "On the Measurement of High-Energy Tau Neutrinos with IceCube"

maybe I want a figure for this, or not so important? (YELLOW)

[37]: Whitehorn et al. (2013), "Penalized splines for smooth representation of high-dimensional Monte Carlo datasets"

[38]: Aartsen et al. (2014), "Energy Reconstruction Methods in the IceCube Neutrino Telescope"

Elaborate whether this is the case (show it in a plot?). Discuss directionality of cascades in general. (ORANGE)

two cascades. Assuming the speed of the HNL to be the speed of light,  $c$ , this already defines the full signature. The HNL particle does not produce any light while traveling, as it is electrically neutral. The full 9 parameters describing the event are  $\Theta = (x, y, z, t, \theta, \phi, E_0, E_1, L)$ . To compute the full likelihood the term in Equation 2.1 is summed over both cascade parts,  $i$ , as  $\sum_i \ln(L_i)$ .

### 2.1.2 Optimization for Low Energy Events

Optimizing the double cascade reconstruction for low energetic events was done in parallel to the development of the model dependent simulation generator introduced in Section ???. A preliminary sample of HNL events was used, containing a continuum of masses between 0.1 GeV and 1.0 GeV and lab frame decay lengths sampled uniformly in the range from 5 m to 500 m. Even though this sample is not representative of a physically correct model and therefore not useful to predict the event expectation, it can still be used to optimize the reconstruction. The double cascade nature of the individual events and the evenly spaced decay length distribution are especially useful for this purpose.

The simulation is processed up to Level 5 of the selection chain described in Section ?? and one of the reconstructions from [39] is applied to the events, fitting a cascade and a track and cascade hypothesis. The results from this reconstruction are used as an input for the double cascade reconstruction, where the position of the vertex, the direction of the event, and its interaction time are used as the input quantities for the first cascade, and the length of the track reconstruction is used as a seed for the distance between the two cascades.

#### Decay Length Seeds

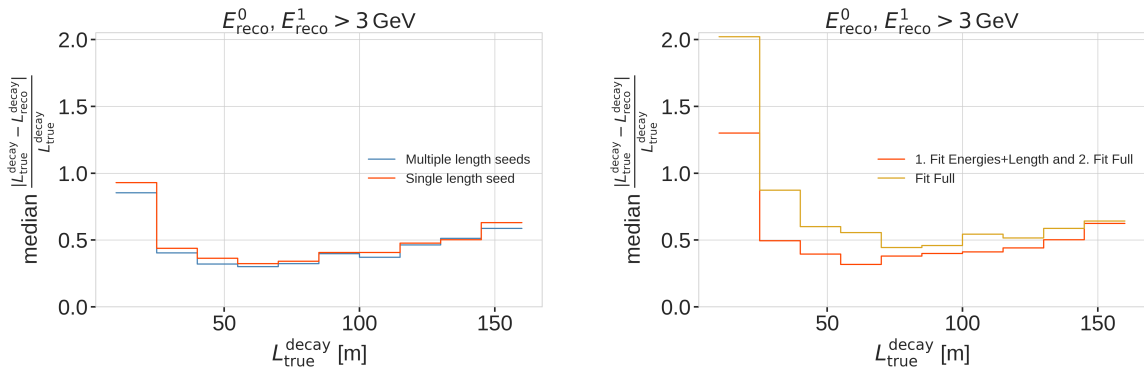


Figure 2.1

fix caption of this figure  
(RED)

The full 9 dimensional likelihood space is very complex and can have many local minima, depending on the specific event and its location in the detector. Especially the seed value of the length between the two cascades was found to have a very strong impact on whether the global minimum was found during the minimization. To mitigate this effect, multiple fits are performed, seeding with variations of the input length at different orders of magnitude. The best result is used, selected based on the total likelihood value of the

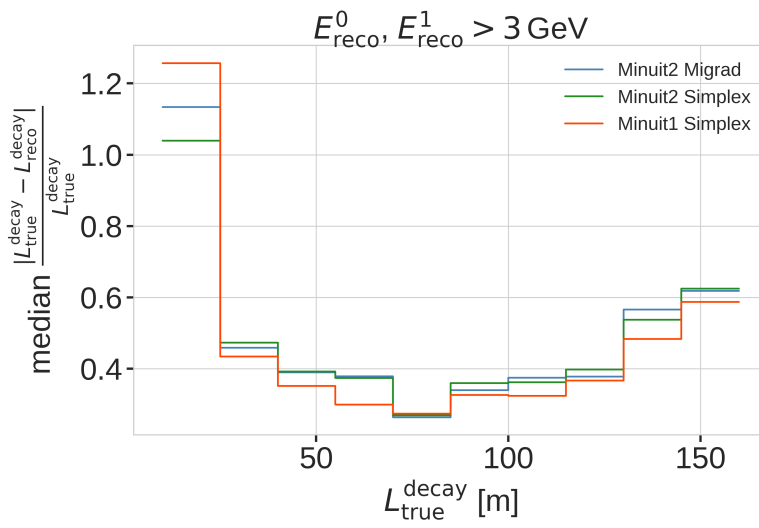
best fit parameter set. A small improvement in the decay length resolution can be found by using this approach as compared to a single length seed. The effect can be seen in the left part of Figure 2.1, which shows the median, absolute, fractional decay length resolution.

### Fit Routine

Because the length seed showed to have such a large impact on the reconstruction performance, a more sophisticated fit routine, than just fitting all 9 parameters at once, was tested. In a first fit iteration, some parameters are fixed and the resulting best fit point is used to fit all 9 parameters in a second iteration. In the right part of Figure 2.1 it can be seen how a fit split into two consecutive steps, where the first step fits only both cascade energies and the decay length and the second step fits the full 9 parameters, performs better as compared to a single, full 9 parameter fit. The initial seed for both routines is the same.

### Minimizer Settings

To investigate the effect of the minimizer used to find the best fit parameters, the reconstruction was performed using three different minimizers, which were easily accessible within the reconstruction framework. The minimizers used were Minuit1 Simplex, Minuit2 Simplex, and Minuit2 Migrad. The results can be seen in Figure 2.2, where the Minuit1 Simplex minimizer performs best. The initial idea was to test a global minimizer, or a routine that can find the rough position of the global minimum first and then a local minimizer to find the exact minimum, but unfortunately this was not possible with the minimizers available in the framework. From the three tested minimizers, Minuit1 Simplex performed best and was chosen as the default for the reconstruction. The comparison of the decay length resolutions can be seen in Figure 2.2.



fix caption of this figure  
(RED)  
Figure 2.2: title

### 2.1.3 Performance

The chosen reconstruction chain used to test the performance of the detector to observe low energetic double cascades is the following; Minuit1 Simplex is used as the minimizer, the decay length is seeded with 3 different values, 0.5x, 1.0x, and 1.5x the length of the track reconstruction, and the fit routine is split into two steps, where the first step fits the energies and the decay length and the second step fits the full 9 parameters. In the first step, the number of time bins in Equation 2.1 is set to 1, so just the number of photons and their spatial information is used. The second step is seeded with the best results from the first fit and here the number of time bins is chosen such that each photon falls into a separate time bin, which means all time information is used. The average runtime per event is  $\sim 16$  s on a single CPU core, but is very dependent on the number of photons observed in the event, since the likelihood calculation in the second step scales with this number and a table lookup has to be performed for each photon.

Describe the results plots here for the first time, so I can come back to the observed features later? Or maybe drop them and just show them later? (RED)

To get a more realistic estimate of the reconstruction performance, it is run on a second preliminary sample of HNL events, containing masses between 0.1 GeV and 3.0 GeV and the lab frame decay length is sampled from an inverse distribution in the range from 1 m to 1000 m, which is a better approximation of the expected exponential decay distribution of the HNL. The performance is shown for events where the reconstruction chain was successfully run, the event selection criteria up to level 7 are fulfilled, and the reconstructed energy of both cascades is above 3.0 GeV. This is done to only investigate well reconstructed events with two significant light depositions at a usual final selection level of the oscillation analyses.

### Energy Resolutions

The energy resolution is inspected by looking at the 2-dimensional distribution of reconstructed energy versus the true energy as shown in Figure 2.3. The bin entries are shown as well as the median and  $\pm 25\%$  calculated per vertical column, to get an idea of the distribution for a given energy slice. The color scale is showing the PDF along in each true energy slice, which is the full information combined into the median $\pm 25\%$  lines. The reconstructed energy is only the energy that is observable from photons, while the true energy is the total cascade energy, including the parts that go into EM neutral particles that do not produce light. It is therefore not expected that the median lines up with the axis diagonal, but rather the reconstructed energy is going to be lower.

The histogram for the first cascade energy is shown on the left and above an energy of  $\sim 10$  GeV the reconstruction performs well, with the median being parallel to the diagonal and the spread in the  $\pm 25\%$  quantile being small. Below this energy the reconstruction is over-estimating the true energy, which is a known effect in IceCube, where the reconstruction is biased towards higher energies around the energy detection threshold, because events that enter the sample are events with an over fluctuation in their light deposition, which makes them pass into the selection and being reconstructible in the first place.

For the second cascade the overall behavior is similar, only that the energy where the reconstruction starts to perform good is higher around  $\sim 20$  GeV.

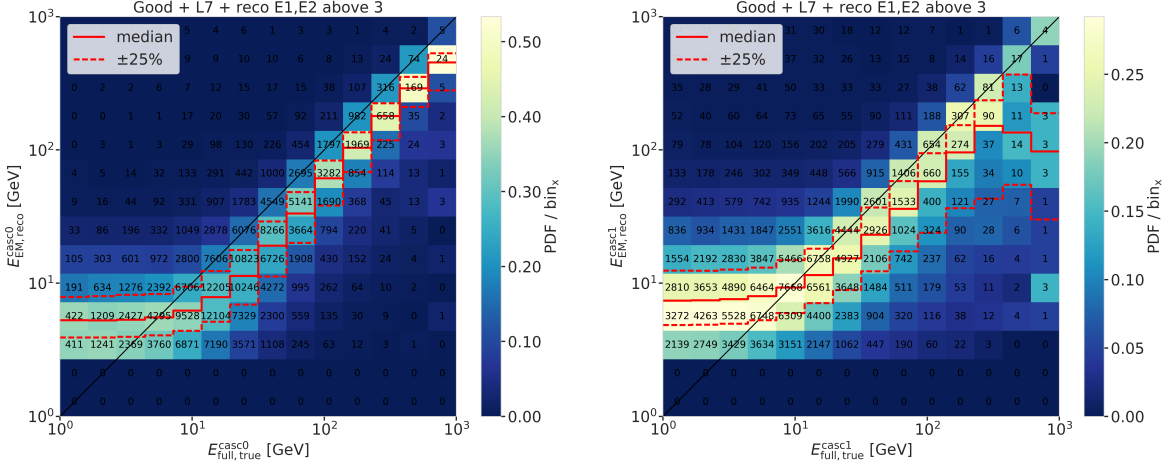


**Figure 2.3:** Reconstructed (EM) energy versus true energy (full) energy for the first cascade (left) and second cascade (right). The color scale is according to the PDF in each vertical true energy slice, with the solid and dashed lines showing the median±25 % quantiles. The bin entries are shown as numbers.

The spread around the median is also larger and starts to expand a lot above 200 GeV, where the statistics are lower as can be seen from the bin counts. It is also very apparent that the majority of energies of the second cascade are at lower true energy values between 1 GeV and 20 GeV.

For both cascade resolutions the effect of the reconstruction being biased towards lower values, due to the comparison of the full true energy to just the reconstructed EM energy can be seen.

## Length Resolutions

### Ideas to write about:

- ▶ explain/reference again the setup of the 2d plots
- ▶ at short true decay lengths, reco always overestimates (why)
- ▶ above 25m, the median reconstruction starts to be almost unbiased up to 80m, but the spread starts to increase towards lower reco lengths
- ▶ but then the median resolution starts to fall below the diagonal and a large population of events which have a very short reconstructed starts to dominate completely above 150m
- ▶ there is still some events that line up with the diagonal, but it is only a small fraction
- ▶ the assumption for the badly reconstructed population is, that for those events only one cascade was observed with enough light and could therefore be reconstructed
- ▶ increasing the minimum cascade energy to 10 GeV already improves the resolution a lot, as can be seen in the right part of the figure, where the median resolution now aligns with the expectation between 40 and 160m, but the spread towards lower reco lengths is still very large and above 200 meters the badly reconstructed population starts to dominate again

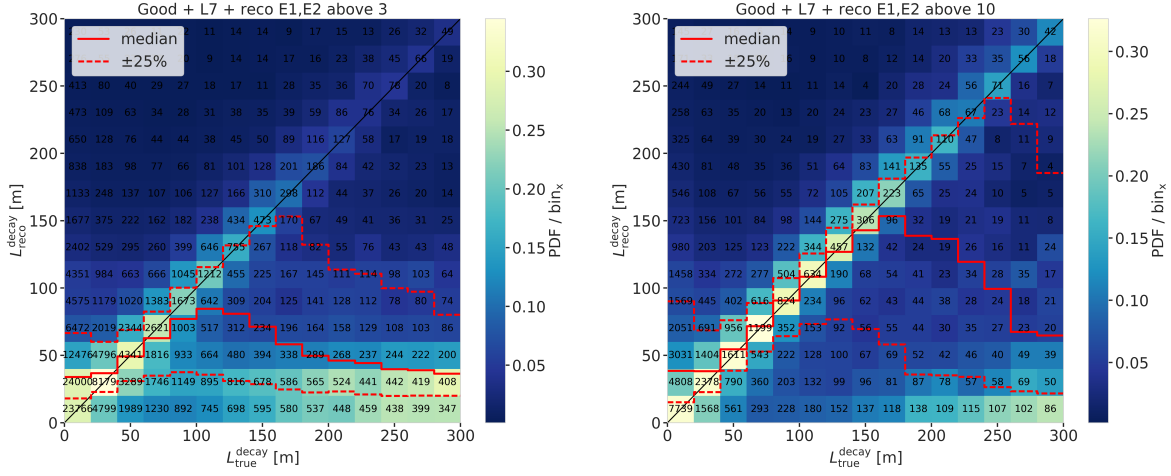
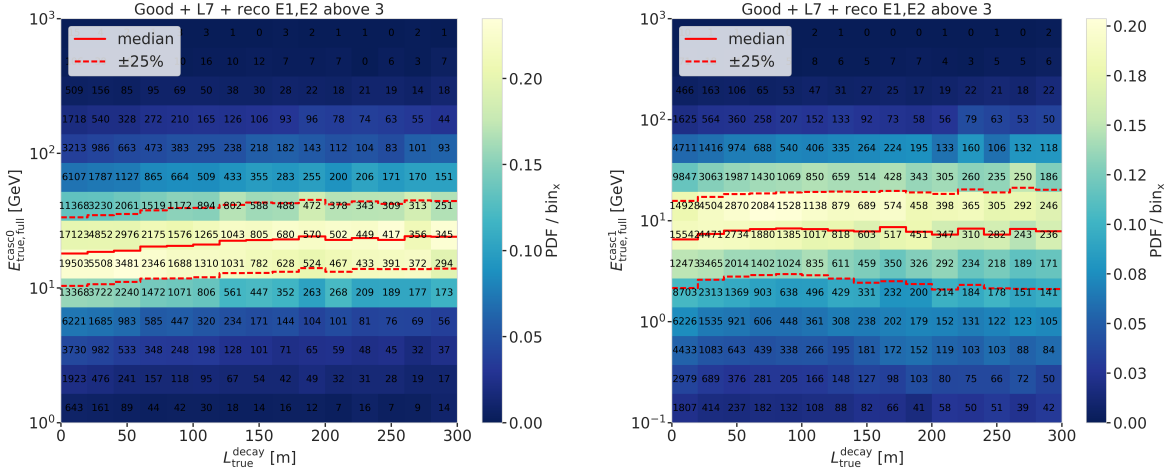


**Figure 2.4:** Reconstructed decay length versus true decay length for a  $\sim 3\text{ GeV}$  (left) and  $\sim 10\text{ GeV}$  (right) minimum reconstructed cascade energies. The color scale is according to the PDF in each vertical true length slice, with the solid and dashed lines showing the median  $\pm 25\%$  quantiles. The bin entries are shown as numbers.

### Badly Reconstructed Cascade Population

#### Ideas to write about:

- ▶ Show/highlight 2d decay length resolution again, basically 2 populations at higher energies
- ▶ only looking at events with  $>10\text{ GeV}$  instead of  $>3\text{ GeV}$  already improves the resolution a lot (low energy and therefore low light is a problem)
- ▶ take a closer look at those populations to find out what's going on
- ▶ multiple things were checked (bad direction (possibly due to seed), cascade position in DC, energies)
- ▶ the direction is worse for the badly reconstructed population, which could be due to a bad seed direction
- ▶ the events are a little further out radially, where the string/DOM spacing is not so tight, which also leads to less light being observed
- ▶ the energy of the second cascade is much lower than the first
- ▶ conclusion: it's a combination of all of them, but the main problem is the low energy
- ▶ true energies vs true length shows that first cascade energies are much larger than second (pick benchmark lengths and state the values!)



## 2.2 Double Cascade Classification

### Missing Points

- ▶ MuMillipede "reconstruction" (depending on how deep I want to go into the classifier I tested?)
- ▶ Calculated variables to input the classifier (distributions?)
- ▶ cuts applied to make sure the classifier is trained on well reconstructed events
- ▶ Tested classifier (BDT) versions and their performance
- ▶ takeaway

## 2.3 Cross Checks

### 2.3.1 Simplistic Sets

From HNL Note, re-write/change (RED)

After generation the events are processed with standard Photon, Detector, L1, and L2 processing and then Taupede+MuMillipede is run on top of the L2 files. Multiple versions with different parameters were produced, some with the OscNext baseline parameters, some without detector noise (in Det level) and some with h2-50cm holeice model, to match the holeice model that was used to generate the photonics tables.

**BrightDom Cleaning** To investigate the effect of the BrightDom cleaning cut the 194601 sample without detector noise (and baseline hole ice model) is used. The BrightDom cleaning is needed to stop a few DOMs with many photon hits to drive the reconstruction because this leads to large biases in the energy estimations. Historically, the BrightDom cleaning was removing all DOMs that had a charge larger than 10 times the mean charge. After quickly checking some charge distributions and how the mean behaves it was clear that the cut should better be defined based on a metric that is less affected by outliers, like the median. Figure ?? shows where the mean and the median are located for an example event. The cut was re-defined to use the median instead of the mean and 10% of the simulation were processed

with [Taupede](#) using 30x and 100x the median as BrightDom cutoff. Figure ?? shows where these values fall for the same example event.

As a quick check of the performance of both cuts the decay length resolution/bias and the resolutions/biases of all energies were checked. The reconstructed decay length is almost not affected by applying this cut, which is as expected, because it is mostly dependent on the arrival time of the photons. The effect on the reconstructed energy is much stronger, where a looser cut (100x) shows a significantly larger bias than the tighter cut at (30x). Even though this was not a highly sophisticated optimization of the BrightDom cut, an improvement was achieved by changing from mean to median and selecting the tighter cut (of the two tested). It's hard to tell how this would perform for high energy events, but I'm quite certain that a definition based on the median would be more reliable than on the mean.

## 2.4 Performance

### 2.4.1 Energy/Decay Length Resolution

describe the "good fit" selection when I first show plots that use it (ORANGE)

add some 1D resolution plots (ORANGE)

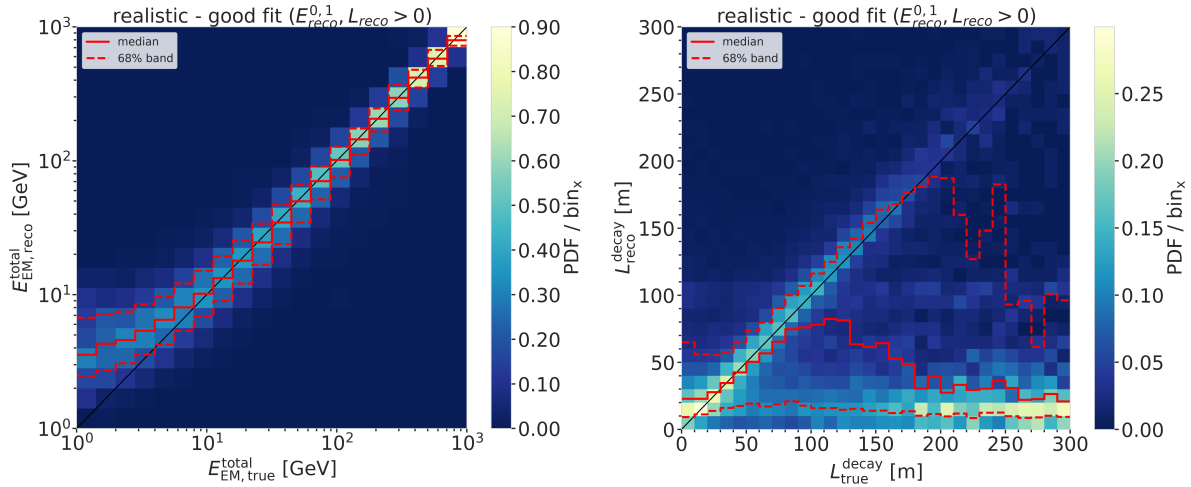
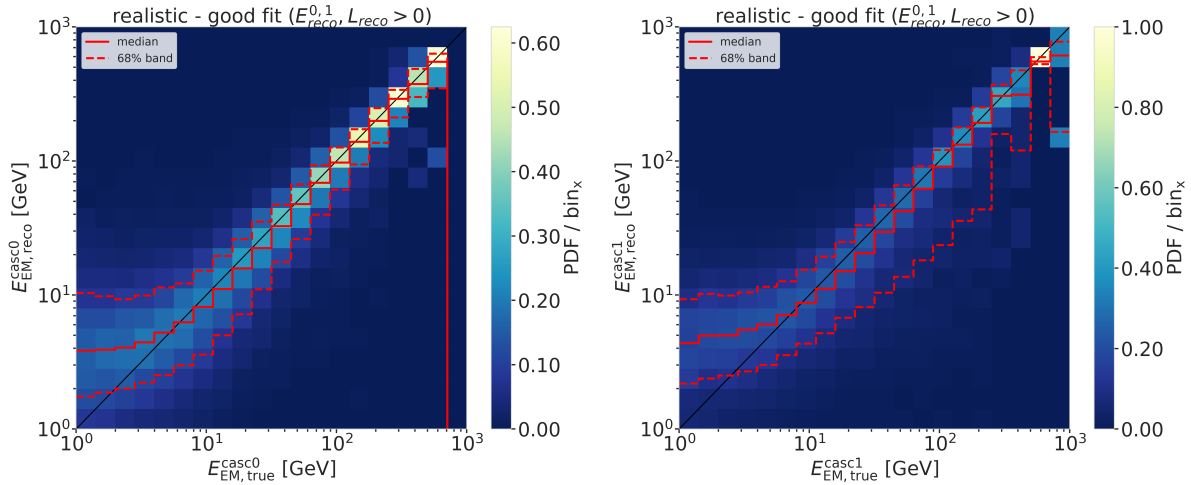
#### 2-D Histograms

Things to mention about the 2d-hists:

- ▶ total energy resolution looks very good, above 10 GeV it's almost unbiased and the 1-sigma resolution band is below 20 %
- ▶ individual cascade resolutions mirror this behavior, but are starting to stabilize in energy at lower energies around 5 GeV to 6 GeV with a broader resolution band of 50 %, but reducing drastically with increasing energy (down to 20 % at 100 GeV)
- ▶ interestingly, the second cascade energy reconstruction performs slightly worse, although they have the same energy ranges. This could hint at an asymmetry in the reconstruction process (might relate to how the two cascades are parameterized) or be due to the different positions and the dominantly up-going direction used in the sampling combined with the DOMs looking down (relate this to the sampling distributions explained/shown in the previous chapter)
- ▶ the decay length resolution looks much worse. In the region between 20 m and 80 m it's roughly unbiased, but 1-sigma resolution band is quite wide with a lot of outliers towards short reconstructed lengths. Below 20 m the reconstructed lengths are always over-estimating the true and above 80 m a population of events start to dominate where the decay lengths isn't getting reconstructed at all, which might indicate that one of the cascades wasn't observers. (Relate to the fact that this marginalizes over all energies, meaning also all events which have one cascade with very low energy are included here.)
- ▶ another interesting feature is the band of reconstructed lengths around 100 m, which is probably related to the spacing between most of the strings, which favors the reconstruction to be around this value, because that's the distance at which light can be observed, just from the fact that the DOMs are spaced at this distance (for low energetic cascades, this can dominate the reconstruction)

fix caption of this figure (RED)

fix caption of this figure (RED)

**Figure 2.5****Figure 2.6**

## Energy Resolution

### Things to mention about the energy resolution:

- Here it can be seen more clearly how the median total energy resolution starts to stabilize around 0.0 at 10 GeV, while for lower energies the reconstruction is over-estimating the true energy. This is a known behavior of energy reconstructions in IceCube, which is mainly due to a selection effect. Only events with a certain amount of light can be reconstructed, which means that the ones with true small energies that are still in the sample are events with over average light production due to fluctuations or other effects?

 fix caption of this figure  
(RED)

## Decay Length Resolution

### Things to mention about the decay length resolution:

- As already mentioned before, the decay length resolution is much worse than the energy resolutions. Figure 2.8 also shows that the

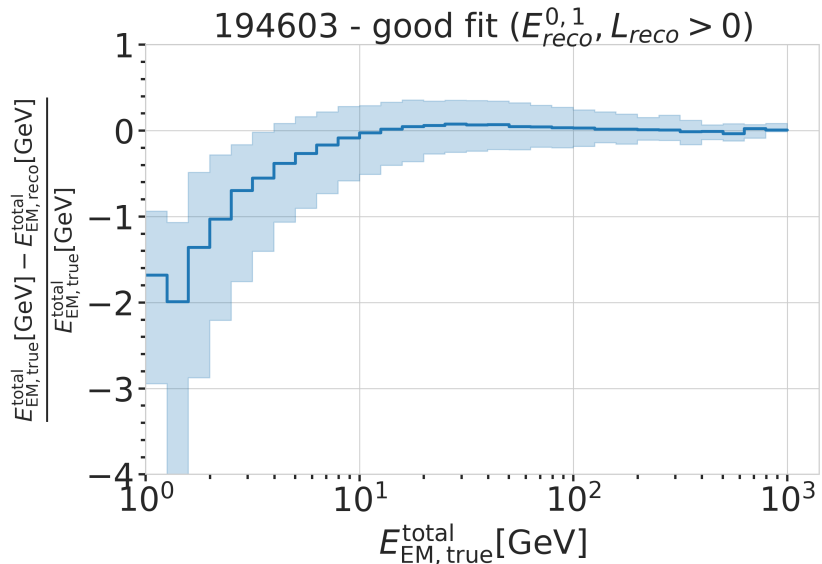


Figure 2.7

median is below 0.0 for short true length and above 0.0 and approaching 1.0 for long true lengths.

- ▶ To investigate whether this is really due to the fact that one of the cascades is not observed, the decay length resolution was plotted against the total energy of the event and the minimum energy of the two cascades Figure 2.9.
- ▶ It can be seen that the median of the decay length resolution stabilizes at 0.0 for a total energy above 20 GeV, but the spread of the distribution is still quite large with a 1-sigma band of 80 % to 100 %.
- ▶ From the plot against the minimum energy it can be seen that the decay length resolution starts to be unbiased for a minimum energy of the cascades of 7 GeV, with an equivalently large spread.
- ▶ A preliminary takeaway from this is that the decay length reconstruction is not reliable at all for events with a total energy below 20 GeV or a minimum cascade energy below 7 GeV.

fix caption of this figure  
(RED)

fix caption of this figure  
(RED)

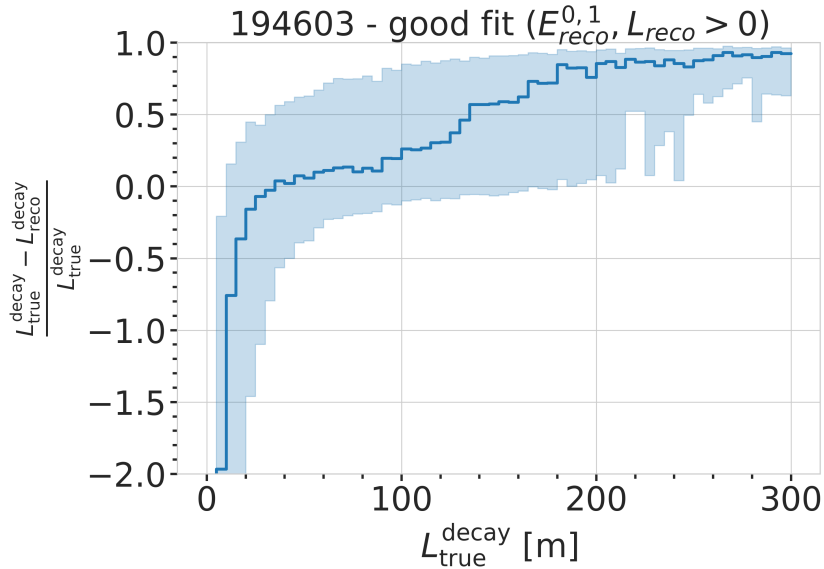


Figure 2.8

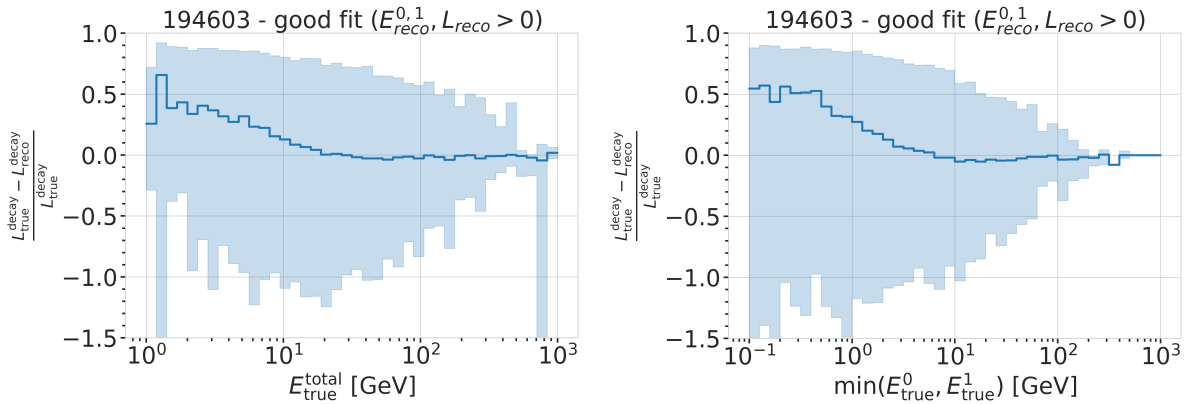


Figure 2.9

## 2.5 Low Energy Event Selection Efficiency

### Discussion ideas:

- ▶ At which level does the selection reduce the HNL the most?
- ▶ Is there a place to improve the HNL selection? (Might have to factor in the BG efficiency, as well..)
- ▶ What of this might change with Upgrade? (maybe rather for the discussion)

Make plot to show efficiency of the OscNext selection for HNL events. (ORANGE)



# Search for an Excess of Heavy Neutral Lepton Events

# 3

The measurement performed in this thesis is the search for an excess of HNL events in the 10 years of IceCube DeepCore data. In principle the two physics parameters to be probed are the mass of the HNL,  $m_4$ , and the mixing between the fourth heavy mass state and the SM  $\tau$  sector,  $|U_{\tau 4}|^2$ . Since the mass itself influences the production and decay kinematics of the event and the accessible decay modes, individual mass samples were produced as described in Section ???. IceCube DeepCore is suited to measure the excess which appears around and below 20 GeV, due to its production from the atmospheric tau neutrinos, although a reduced lower energy threshold might improve the analysis. The measurement will be performed for the three mass samples individually, while the mixing is the parameter that can be varied continuously and will be measured in the fit.

## 3.1 Final Level Sample

The final level sample of this analysis always consists of the neutrino and muon MC introduced in Section ?? and one of the three HNL samples explained in Section ???. All of those simulation sets and the 10 years of IceCube DeepCore data are processed through the full processing and event selection chain described in Section ?? and Section ?? leading to the final level sample. Since applying the final cuts from Section ?? leaves an insignificant amount of pure noise events in the sample, the noise simulation is not included in the analysis and will not be listed here.

### 3.1.1 Expected Rates/Events

The rates and the expected number of events for the SM background are shown in Table 3.1 with around 175000 total events expected in the 10 years. The explicit, good detector livetime in this data taking period is 9.28 years. The rates are calculated by summing the weights of all events in the final level sample, while the uncertainties are calculated by taking the square root of the sum of the weights squared. The expected number of events is calculated by multiplying the rate with the livetime. The individual fractions show that this sample is neutrino dominated where the majority of events are  $\nu_\mu$ -CC events.

3.1	Final Level Sample . . . . .	27
3.2	Statistical Analysis . . . . .	28
3.3	Analysis Checks . . . . .	31
3.4	Results . . . . .	32

add information about the matter profile used (ORANGE)

add information about the oscillation probability calculation and the software used for it (RED)

Type	Rate [mHz]	Events (in 9.28 years)	Fraction [%]
$\nu_\mu^{\text{CC}}$	0.3531	$103321 \pm 113$	58.9
$\nu_e^{\text{CC}}$	0.1418	$41490 \pm 69$	23.7
$\nu_{\text{NC}}$	0.0666	$19491 \pm 47$	11.1
$\nu_\tau^{\text{CC}}$	0.0345	$10094 \pm 22$	5.8
$\mu$	0.0032	$936 \pm 15$	0.5
total	0.5991	$175336 \pm 143$	100.0

**Table 3.1:** Final level rates and event expectation of the SM background particle types.

Table 3.2 shows the rates and expected number of events for the HNL signal simulation. The expectation depends on the mass and the mixing and shown

Should I adapt the total numbers to match the sum of the rounded individual parts? (YELLOW)

here are two example mixings for all the three masses that are being tested in this work. A mixing of 0.0 would result in no HNL events at all. It can already be seen that for the smaller mixing of  $|U_{\tau 4}|^2 = 10^{-3}$  the expected number of events is very low, while at the larger mixing of  $|U_{\tau 4}|^2 = 10^{-1}$  the number is comparable to the amount of muons in the background sample.

**Table 3.2:** Final level rates and event expectations of the HNL signal for all three masses and two example mixing values.

HNL mass	Rate [μHz]	Events (in 9.28 years)
$ U_{\tau 4} ^2 = 10^{-1}$		
0.3 GeV	$3.3298 \pm 0.0053$	$974.5 \pm 1.6$
0.6 GeV	$3.0583 \pm 0.0058$	$895.0 \pm 1.7$
1.0 GeV	$2.4988 \pm 0.0059$	$731.3 \pm 1.7$
$ U_{\tau 4} ^2 = 10^{-3}$		
0.3 GeV	0.0057	$1.67 \pm 0.01$
0.6 GeV	0.0220	$6.44 \pm 0.01$
1.0 GeV	0.0248	$7.27 \pm 0.01$

### 3.1.2 Analysis Binning

[40]: Yu et al. (2023), "Recent neutrino oscillation result with the Ice-Cube experiment"

The identical binning to the analysis performed in [40] is used. It was chosen such that the track-like bin has the largest  $\nu_\mu$ -CC fraction. Extending the binning towards lower energies or increasing the number of bins in energy or cosine of the zenith angle did not improve the HNL sensitivities significantly. It also has to be considered that sufficient data events need to end up in the individual bins to result in a good fit, which was already investigated in the previous analysis. To mitigate the low data statistics, a few bins were not taken into account in the analysis. There are three bins in PID (cascade-like, mixed, and track-like), 12 bins in reconstructed energy, and 8 bins in cosine of the reconstructed zenith angle as specified in Table 3.3. Originally, there were two more bins in  $\cos(\theta)$ , which were removed to reduce muons coming from the horizon and some low energy bins in the cascade-like bin are removed due to the low event statistics.

**Table 3.3:** Three dimensional binning used in the analysis. All variables are from the HEDRENN reconstruction explained in Section ??.

Add fractions of the different particle types in the bins for benchmark mass/mixing (another table?) (ORANGE)

[41]: Aartsen et al. (2020), "Computational techniques for the analysis of small signals in high-statistics neutrino oscillation experiments"

Do I want more information about the different pipelines and stages?  
Could link back to the extra stage I wrote and add the earth model and oscillation calculation information here, I guess?!  
(ORANGE)

Variable	N <sub>bins</sub>	Edges	Step
P <sub>v</sub>	3	[0.00, 0.25, 0.55, 1.00]	linear
E	12	[5.00, 100.00]	logarithmic
cos(θ)	8	[-1.00, 0.04]	linear

## 3.2 Statistical Analysis

### 3.2.1 Low Energy Analysis Framework

The analysis is performed using the PISA [41] [42] software framework, which was developed to perform analyses "of small signals in high-statistics neutrino oscillation experiments". It is used to generate the expected event distributions from several MC samples, which can then be compared to the observed data. The expectation for each sample is calculated in parallel, applying physics and nuisance parameter effects in a stage-wise manner, before combining the final expectation from all the samples.

### 3.2.2 Test Statistic

The measurements are performed by comparing the weighted MC to the data. Through variation of the nuisance and physics parameters that govern the weights, the best matching set of parameters can be found. The comparison is done using a modified  $\chi^2$  defined as

$$\chi_{\text{mod}}^2 = \sum_{i \in \text{bins}} \frac{(N_i^{\text{exp}} - N_i^{\text{obs}})^2}{N_i^{\text{exp}} + (\sigma_i^v)^2 + (\sigma_i^{\mu})^2 + (\sigma_i^{\text{HNL}})^2} + \sum_{j \in \text{syst}} \frac{(s_j - \hat{s}_j)^2}{\sigma_{s_j}^2}, \quad (3.1)$$

as the *test statistic (TS)*. The total even expectation is  $N_i^{\text{exp}} = N_i^v + N_i^{\mu} + N_i^{\text{HNL}}$ , where  $N_i^v$ ,  $N_i^{\mu}$ , and  $N_i^{\text{HNL}}$  are the expected number of events in bin  $i$  from neutrinos, atmospheric muons, and HNLs, while  $N_i^{\text{obs}}$  is the observed number of events in bin  $i$ . The expected number of events from each particle type is calculated by summing the weights of all events in the bin  $N_i^{\text{type}} = \sum_i^{\text{type}} \omega_i$ , with the statistical uncertainty being  $(\sigma_i^{\text{type}})^2 = \sum_i^{\text{type}} \omega_i^2$ . The additional term in Equation 3.1 is included to apply a penalty term for prior knowledge of the systematic uncertainties of the parameters where they are known.  $s_j$  are the systematic parameters that are varied in the fit, while  $\hat{s}_j$  are their nominal values and  $\sigma_{s_j}$  are the known uncertainties.

I feel like I have to be a bit more precise on what is the fit metric (e.g. the mod chi2) and what is the TS, as in the mod chi2 difference, which is the actual TS, right? (RED)

Do I want/need to include the description of the KDE muon estimation? (YELLOW)

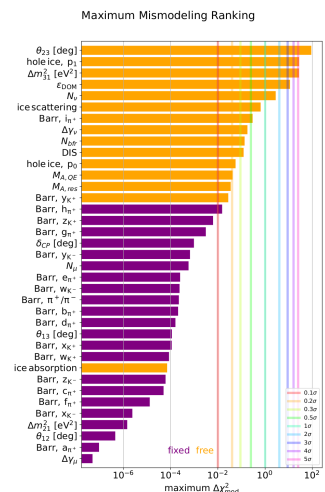


Figure 3.1: "calculated at a mixing of 0.1 and for the 1.0 GeV sample"

### 3.2.3 Physics Parameters

The variable physics parameter in this analysis is the mixing between the HNL and the SM  $\tau$  sector,  $|U_{\tau 4}|^2$ . It can be changed continuously in the range of  $[0.0, 1.0]$  by applying the weighting scheme described in Section ???. The fit is initialized at an off-nominal value of 0.1. The other physics parameter, the mass  $m_4$  of the HNL, is fixed to one of the three discrete masses to be tested, by using the corresponding sample of the HNL simulation described in Section ???.

### 3.2.4 Nuisance Parameters

To decide which systematic uncertainties should be included in the fit, we test the potential impact they have on the TS if they are neglected. The test is performed by creating Asimov data using the 1.0 GeV sample at a mixing value of 0.1, which is around the value where the analysis starts to become sensitive. The systematic parameter of interest is set to a value above its nominal expectation, either pulled up by  $+1\sigma$  or by an educated estimate for parameters without a well-defined uncertainty. A fit is performed fixing the systematic parameter of interest and leaving all additional parameters free. The resulting TS is the mis-modeling significance between this fit and a fit with all parameters free, which would result in a TS of 0.0 for this Asimov test. Parameters below a significance of  $0.1\sigma$  are fixed and the test is performed in an iterative manner until the final set of free parameters is found. Figure 3.1 shows the resulting significances of one of these tests. In the final selection of free parameters the Barr  $h_{\pi^+}$  parameter was also left free and the ice absorption is still kept free, despite showing a small significance. This is done because the bulk ice parameters are not well constrained and are known to have a large impact, which might be concealed in the test, due to correlations with the other parameters.

Blow up labels/legend/title and make it more readable in the margin or move it into the main text? (RED)

I don't like this formulation, but don't know better right now.. (YELLOW)

elaborate why this is also done to cover the whole energy range for the pion production, referencing the Barr Block plot that I haven't included yet :D (RED)

I truly dislike this sentence, too, better ideas? (YELLOW)

**Table 3.4:** Systematic uncertainty parameters that are left free to float in the fit. Their allowed fit ranges are shown with the nominal value and the Gaussian prior width if applicable.

Parameter	Nominal	Range	Prior
$\Delta\gamma_\nu$	0.0	[-0.5, 0.5]	0.1
Barr $h_{\pi^+}$	0.0	[-0.75, 0.75]	0.15
Barr $i_{\pi^+}$	0.0	[-3.05, 3.05]	0.61
Barr $y_{K^+}$	0.0	[-1.5, 1.5]	0.3
$\theta_{23} [\circ]$	47.5047	[0.0, 90.0]	-
$\Delta m_{31}^2 [\text{eV}^2]$	0.002475	[0.001, 0.004]	-
DIS	0.0	[-0.5, 1.5]	1.0
$N_\nu$	1.0	[0.1, 2.0]	-
$\epsilon_{\text{DOM}}$	1.0	[0.8, 1.2]	0.1
hole ice $p_0$	0.101569	[-0.6, 0.5]	-
hole ice $p_1$	-0.049344	[-0.2, 0.2]	-
bulk ice absorption	1.0	[0.85, 1.15]	-
bulk ice scattering	1.05	[0.9, 1.2]	-
$N_{\text{bfr}}$	0.0	[-0.2, 1.2]	-
$M_{A,\text{QE}}$	0.0	[-2.0, 2.0]	1.0
$M_{A,\text{res}}$	0.0	[-2.0, 2.0]	1.0

I'm just writing out the data from the table, but I need to mention/motivate the included priors here and maybe just point to the table for the ranges/nominal values? (Not quite sure about this) (RED)

[43]: Evans et al. (2017), "Uncertainties in atmospheric muon-neutrino fluxes arising from cosmic-ray primaries"

say something about their priors (RED)

say something about their priors (RED)

[44]: Feintzeig (2014), "Searches for Point-like Sources of Astrophysical Neutrinos with the IceCube Neutrino Observatory"

[45]: Kulacz (2019), "In Situ Measurement of the IceCube DOM Efficiency Factor Using Atmospheric Minimum Ionizing Muons"

cite?! (ORANGE)

I should add some final level effects of some systematics on the 3D binning and maybe discuss how they are different from the signal shape, or so? (ORANGE)

The scaling parameter  $N_\nu$  is included to account for the unknown overall normalization of the neutrino rate. It has the identical effect on the SM neutrino events and the BSM HNL events and its nominal value is set to 1.0 with a wide range of [0.1, 2.0].

Concerning the atmospheric neutrino flux, the CR power law flux correction factor  $\Delta\gamma_\nu$  is included with nominal value of 0.0 and a range of [-0.5, 0.5]. The nominal value corresponds to a CR power law of  $E^{-2}$  and a slightly conservative prior of 0.1 is applied to the parameter, while latest measurements have an uncertainty of 0.05 [43].

Additionally, the Barr  $h_{\pi^+}$ , Barr  $i_{\pi^+}$ , and Barr  $y_{K^+}$  parameters of the pion and kaon production uncertainties are included with nominal values of 0.0 and ranges of [-0.75, 0.75], [-3.05, 3.05], and [-1.5, 1.5], respectively.

From the cross-section uncertainties introduced in Section ??, all three parameters, DIS,  $M_{A,\text{QE}}$ , and  $M_{A,\text{res}}$  are included in the fit with nominal values of 0.0 for all of them and range [-0.5, 1.5] for DIS and [-2.0, 2.0] for the axial mass parameters  $M_{A,\text{QE}}$ , and  $M_{A,\text{res}}$ .

All the detector systematic uncertainties are included in the fit. The DOM efficiency  $\epsilon_{\text{DOM}}$  has a nominal value of 1.0 and a range of [0.8, 1.2]. It is constrained by a Gaussian prior with a width of 0.1, which is a conservative estimate based on the studies of the optical efficiency using minimum ionizing muons from [44, 45]. The hole ice model parameters  $p_0$  and  $p_1$  are included with nominal values of 0.101569 and -0.049344, respectively, and ranges of [-0.6, 0.5] and [-0.2, 0.2]. The bulk ice absorption and scattering parameters are included with nominal values of 1.0 and 1.05, respectively, and ranges of [0.85, 1.15] and [0.9, 1.2]. They are unconstrained in the fit and the ranges are set to be conservative determined from calibration data

The two atmospheric neutrino oscillation parameters  $\theta_{23}$  and  $\Delta m_{31}^2$  are also included in the fit with nominal values of  $47.5047^\circ$  and  $2.475 \times 10^{-3} \text{ eV}^2$ , respectively. Since they govern the shape and the strength of the tau neutrino flux, by defining the oscillation from  $\nu_\mu$  to  $\nu_\tau$ , they are also relevant for the HNL signal shape. Their ranges are set to  $[0.0^\circ, 90.0^\circ]$  and  $[0.001 \text{ eV}^2, 0.004 \text{ eV}^2]$ .

### 3.3 Analysis Checks

Fitting to data will be performed in a *blind* manner, where the analyzer does not immediately see the fitted physics and nuisance parameter values, but first checks that a set of pre-defined *goodness of fit* (GOF) criteria are fulfilled. At this point changes to the analysis can still be made, if the criteria are not met. This is done to circumvent the so-called *confirmation bias* [46], where the analyzer might be tempted to construct the analysis in a way that confirms their expectation. After the GOF criteria are met to satisfaction, the fit results are unblinded and the full result can be revealed. Before these blind fits to data are performed, the robustness of the analysis method is tested using pseudo-data that is generated from the MC.

[46]: Nickerson (1998), "Confirmation Bias: A Ubiquitous Phenomenon in Many Guises"

#### 3.3.1 Minimization Robustness

To find the set of parameters that describes the data best, a staged minimization routine is used. In the first stage, a fit with coarse minimizer settings is performed to find a rough estimate of the *best fit point* (BFP). In the second stage, the fit is performed again in both octants<sup>1</sup> of  $\theta_{23}$ , starting from the BFP of the coarse fit. For each individual fit the MIGRAD routine of IMINUIT [47] is used to minimize the  $\chi^2_{\text{mod}}$  TS defined in Equation 3.1. Iminuit is a fast, python compatible minimizer based on the MINUIT2 C++ library [48]. The individual minimizer settings for both stages are shown in Table 3.5.

To test the minimization routine and to make sure it consistently recovers any injected physics parameters, pseudo-data sets are produced from the MC by choosing the nominal nuisance parameters and specific physics parameters, without adding any statistical or systematic fluctuations to it. These so-called *Asimov*<sup>2</sup> data sets are then fit back with the full analysis chain. This type of test is called *Asimov inject/recover test*. A set of mixing values between  $10^{-3}$  and  $10^0$  is injected and fit back. Even though this range is well within the excluded regions by other experiments, discussed in Section 1.2.3, this covers the current sensitive region of the analysis in IceCube DeepCore. Without fluctuations the fit is expected to always recover the injected parameters (both physics and nuisance parameters). The fitted mixing values from the Asimov inject/recover tests are compared to the true injected values in Figure 3.2 for the 0.6 GeV sample. As expected, the fit is always able to recover the injected phycis parameter and the nuisance paramters. The same is true for the other mass samples and the additional plots for the other mass samples can be found in Section B.1.

1: There is a degeneracy between the lower octant ( $\theta_{23} < 45^\circ$ ) and the upper octant ( $\theta_{23} > 45^\circ$ ), which can lead to TS minima (local and global) at two positions that are mirrored around  $45^\circ$  in  $\theta_{23}$ .

[47]: Dembinski et al. (2022), *scikit-hep/iminuit*: v2.17.0

again, I think fit metric and TS are mixed up a bit (RED)

[48]: James et al. (1975), "Minuit: A System for Function Minimization and Analysis of the Parameter Errors and Correlations"

Fit	Err.	Prec.	Tol.
Coarse	1e-1	1e-8	1e-1
Fine	1e-5	1e-14	1e-5

**Table 3.5:** Migrad settings for the two stages in the minimization routine. Err. are the step size for the numerical gradient estimation, Prec. is the precision with which the LLH is calculated, and Tol. is the tolerance for the minimization.

2: A pseudo-data set without statistical fluctuations is called Asimov data set.

Do I want additional plots for this (fit diff, LLH distr, minim. stats, param. fits)? (YELLOW)

#### 3.3.2 Goodness of Fit

To estimate the GOF, pseudo-data is generated from the MC by injecting the BFP parameters as true parameters and then fluctuating the expected bin counts to account for MC uncertainty and Poisson fluctuations in data. First, the expectation value of each bin is drawn from a Gaussian distribution centered at the nominal expectation value with a standard deviation corresponding to the MC uncertainty of the bin. Based on this sampled expectation value, each bin count is drawn from a Poisson distribution, independently, to get the final pseudo-data set. These pseudo-data sets are then fit back with the analysis chain. By comparing the distribution of TS



**Figure 3.2:** Asimov inject/recover test for the 0.6 GeV mass sample. Mixing values between  $10^{-3}$  and  $10^0$  are injected and fit back with the full analysis chain. The injected parameter is always recovered within the statistical uncertainty.

here again, this is just the fit metric, right? (RED)

Add bin-wise TS distribution? Add 3D TS maps? (RED)

values from this *ensemble* of pseudo-data trials to the TS of the fit to real data, a p-value can be calculated. The p-value is the probability of finding a TS value at least as large as the one from the data fit. Figure 3.3 shows the TS distribution from the ensemble tests for the 0.6 GeV mass sample and the observed TS value from the fit, resulting in a p-value of 28.5 %. The p-values for the 0.3 GeV and 1.0 GeV are 28.3 % and 26.0 %, respectively and the corresponding plots are shown in Section B.2. Based on this test, it is concluded that the fit result is compatible with the expectation from the ensemble of pseudo-data trials.

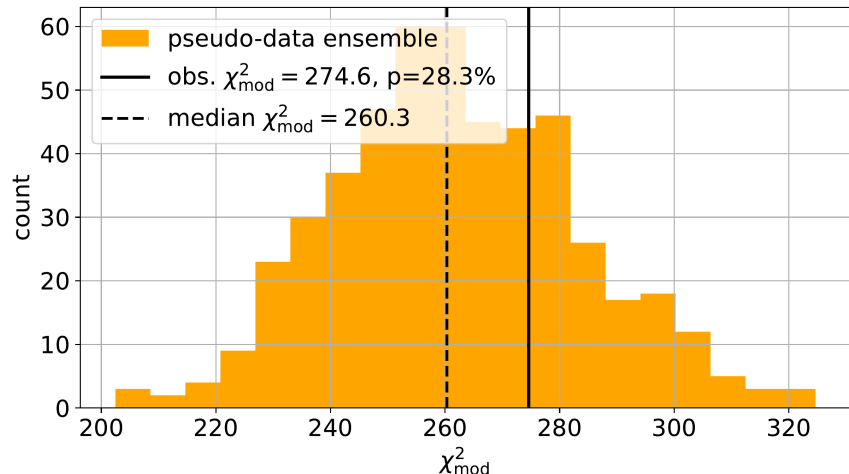


**Figure 3.3:** Observed fit TS and TS distribution from pseudo-data trials for the 0.6 GeV mass sample.

## 3.4 Results

### 3.4.1 Best Fit Nuisance Parameters

The resulting nuisance parameter values from the fits are illustrated in Figure 3.4, where the differences to the nominal values are shown, normalized by the distance to the closest boundary. The results from all three fits are shown in the same plot and the fits prefer values of the same size for all

three mass samples. For parameters that had a Gaussian prior, the  $1\sigma$  range is also displayed. As was already confirmed during the blind fit procedure, all fitted parameters are within this range, but the Barr  $h_{\pi^+}$  parameter is smaller and the Barr  $i_{\pi^+}$  is larger than expected, both being very close within the  $+1\sigma$  and the  $-1\sigma$  range, respectively. The DIS parameter fits to a smaller value than the nominal and all ice parameters, both hole ice  $p_0$ , and  $p_1$  as well as bulk ice absorption, and scattering are found at values lower than the nominal. The effective ice model parameter,  $N_{\text{bfr}}$ , prefers a value of  $\sim 0.74$ , indicating that the data is more *BFR*-like (value of 1.0) than *Spice 3.2.1*-like (value of 0.0). For completeness's sake, the explicit results are listed in Table C.1. There, the nominal values and the absolute differences to the best fit value are also presented.

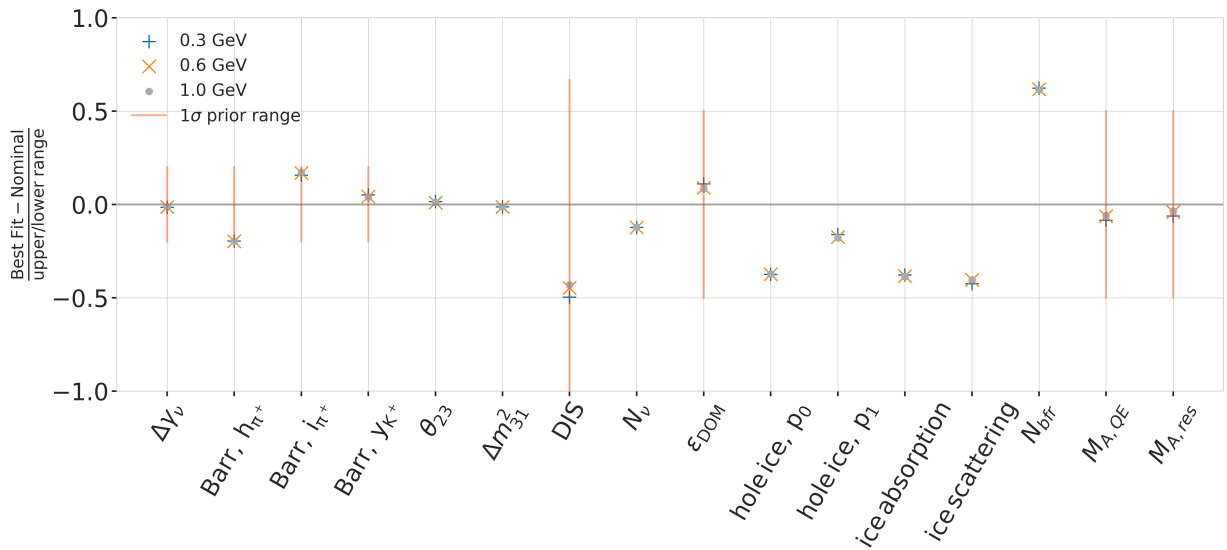


**Figure 3.4:** Best fit nuisance parameter distances to the nominal values, normalized by the distance to the closest boundary. For parameters with a Gaussian prior, the  $+1\sigma$  range is also shown.

### 3.4.2 Best Fit Parameters and Limits

The fitted mixing values are

$$\begin{aligned}|U_{74}|_{\text{BFP}}^2(0.3 \text{ GeV}) &= 0.003^{+0.084}, \\|U_{74}|_{\text{BFP}}^2(0.6 \text{ GeV}) &= 0.080^{+0.134}, \text{ and} \\|U_{74}|_{\text{BFP}}^2(1.0 \text{ GeV}) &= 0.106^{+0.132},\end{aligned}$$

with their  $+1\sigma$  uncertainty. All of them are compatible with the null hypothesis of 0.0 mixing, although the 0.6 GeV and 1.0 GeV fits indicate a mixing value around 0.09. The best fit mixing values and the corresponding upper limits at 68 % and 90 % confidence level (CL) are listed in Table 3.6, also showing the CL at the null hypothesis, which is the probability of excluding the null hypothesis with this fit. The CLs are estimated by assuming that Wilks' theorem [49] holds, meaning that the TS follows a  $\chi^2$  distribution with one degree of freedom.

Figure 3.5 shows the observed likelihood profile for the 0.6 GeV sample, which is the difference in  $\chi^2_{\text{mod}}$  between the best fit and each scan point in  $|U_{74}|^2$ . Also shown is the expected likelihood profile, based on a scan over

sort the variables also by type, same as in the table "best\_fit\_parameters"? (ORANGE)

Show best fit hole ice angular acceptance compared to nominal and flasher/in-situ fits, maybe? (YELLOW)

Discuss what it means that the parameters are at these values? Here, or somewhere else? (RED)

[49]: Wilks (1938), "The Large-Sample Distribution of the Likelihood Ratio for Testing Composite Hypotheses"

fix table caption (RED)

**Table 3.6:** xx

HNL mass	$ U_{\tau 4} ^2_{\text{BFP}}$	68 % CL	90 % CL	NH p-value
0.3 GeV	0.003	0.087	0.194	0.97
0.6 GeV	0.080	0.214	0.355	0.79
1.0 GeV	0.106	0.238	0.396	0.63

fix once I have them produced (RED)

fix once I have the brazil bands (RED)

Asimov data produced at the BFP. The observed CLs are slightly larger/smaller than the expected CL. To ensure this is compatible with random fluctuations, the expected likelihood is also profiled for 100 pseudo-data sets, which are generated at the BFP and then fluctuated using both Poisson and Gaussian fluctuations, to include the data and the MC uncertainty, as was already done for the ensemble tests. The resulting CLs are shown as the colored areas and the observed contour is well within the 68 % band, confirming that it is compatible with data fluctuations. Figure C.1 shows the same likelihood profiles and bands for the other two mass samples. For both of them the observed CLs are also slightly larger/smaller than the expected, but still within the 68 % band of the pseudo-data trials, so they are also compatible with random fluctuations.

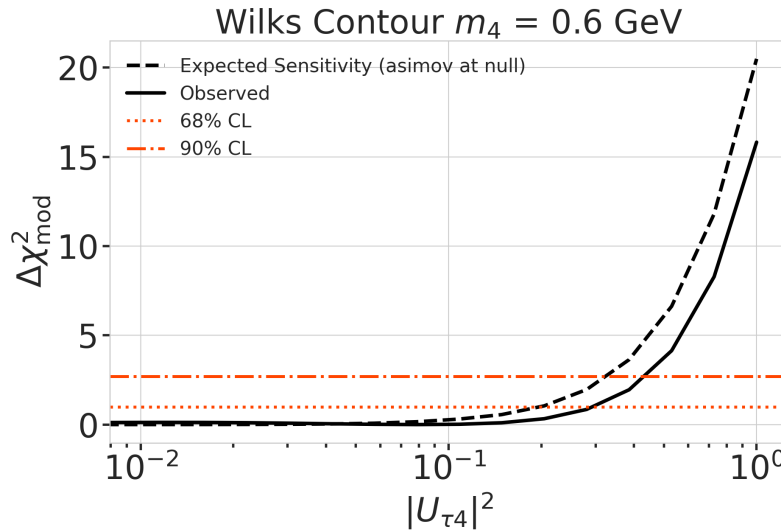


Figure 3.5: xx  
fix caption for this figure (RED)

make plot with BFPs and limit, comparing to upper limits from other experiments, think about how to present it (RED)

specify which they are, once I have them (RED)

add 1-d data/mc agreement for example mass sample (0.6?) and all 3 analysis variables (RED)

add table with reduced chi2 for all 1-d distributions (RED)

### 3.4.3 Data/MC Agreement

At the BFP, the agreement between the data and simulation is probed by comparing the 1-dimensional analysis distributions for PID, energy, and cosine of the zenith angle. As an example, two distributions for the 0.6 GeV mass sample are shown in Figure ???. The data is compared to the total MC expectation, which is also split up into its composing parts. Good agreement can be observed in the pull distributions and is quantified by a reduced  $\chi^2$ , which is close to 1.0 for all distributions. The reduced  $\chi^2$  for all investigated distributions is listed in Table ???, while the distributions themselves can be found in Section ???.

## **APPENDIX**



# A

## Heavy Neutral Lepton Signal Simulation

### A.1 Model Independent Simulation Distributions

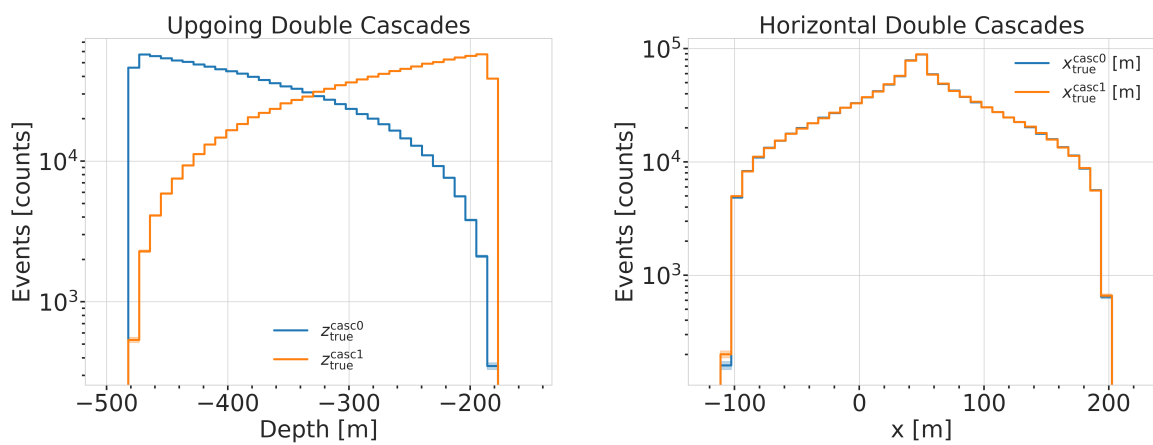


**Figure A.1:** Generation level distributions of the simplistic simulation sets. Vertical positions (left) and horizontal positions (right) of both sets are shown.

- Re-make plot with  $x, y$  for horizontal set one plot!
- Re-make plot with  $x, y, z$  for both cascades in one.
- Re-arrange plots in a more sensible way.

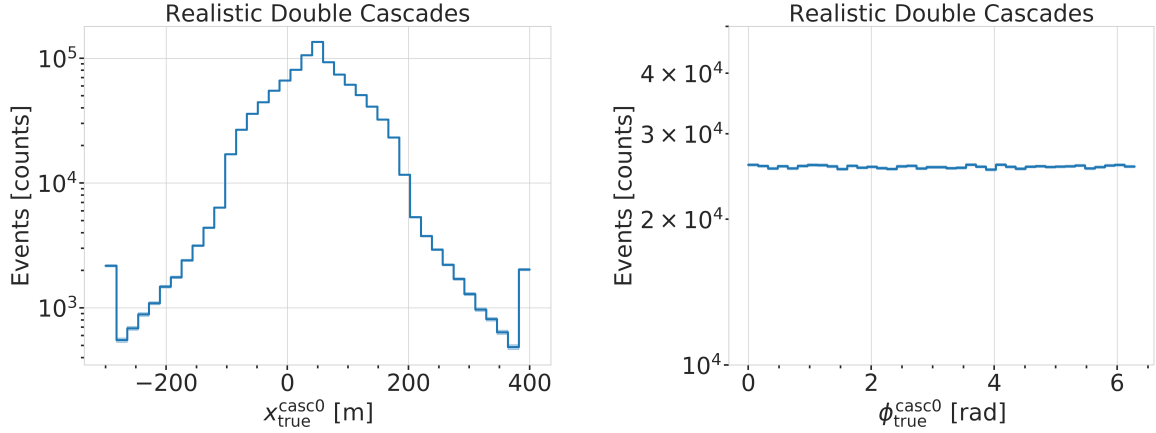


**Figure A.2:** Generation level distributions of the realistic simulation set. Shown are the cascade  $x, y, z$  positions (left) and direction angles (right).

## A.2 Model Dependent Simulation Distributions

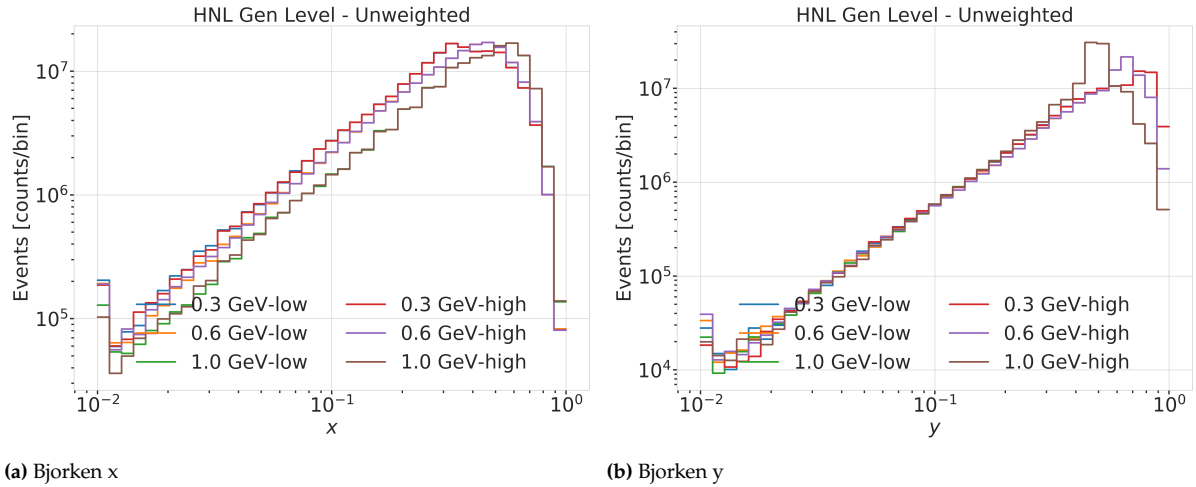


**Figure A.3:** Generation level distributions of the model dependent simulation.

# B

---

## Analysis Checks

---

### B.1 Minimization Robustness

Figure B.1 shows additional Asimov inject/recover tests for the 0.3 GeV and the 1.0 GeV mass sets. The tests were described in Section 3.3.1.

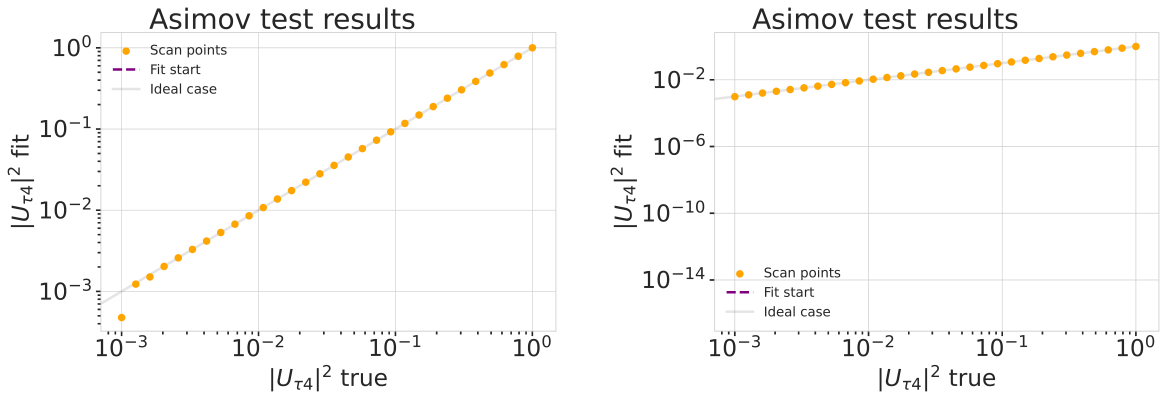


**Figure B.1:** Asimov inject/recover test for the 0.3 GeV (left) and the 1.0 GeV (right) mass sets. Mixing values between  $10^{-3}$  and  $10^0$  are injected and fit back with the full analysis chain. The injected parameter is always recovered within the statistical uncertainty.

### B.2 Ensemble Tests

Figure B.2 shows additional TS distributions from pseudo-data trials and the observed TS from the fit to the data for the ensemble for the 0.3 GeV and the 1.0 GeV mass sets. The tests were described in Section 3.3.2.

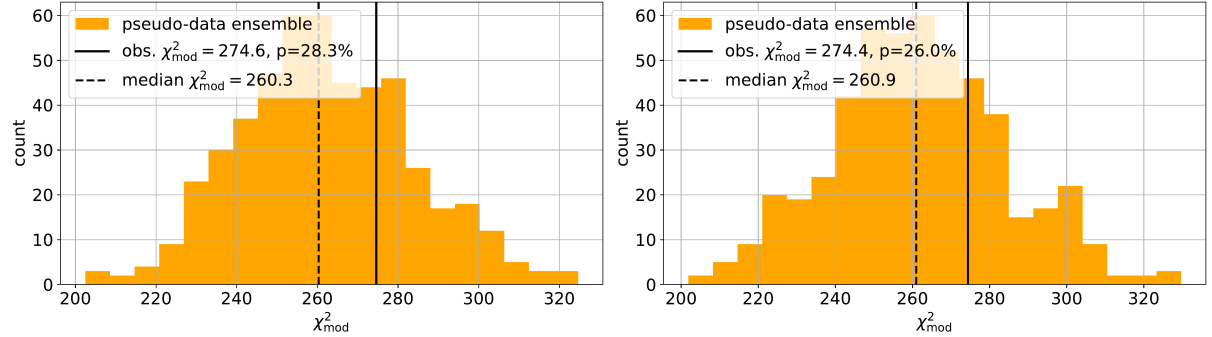


**Figure B.2:** Observed fit TS and TS distribution from pseudo-data trials for the 0.3 GeV (left) and the 1.0 GeV (right) mass set.



# C

---

## Analysis Results

---

### C.1 Best Fit Nuisance Parameters

Table C.1: xx

Parameter	Nominal	Best Fit			Nominal - Best Fit		
		0.3 GeV	0.6 GeV	1.0 GeV	0.3 GeV	0.6 GeV	1.0 GeV
$\Delta\gamma_\nu$	0.000000	-0.007926	-0.006692	-0.006596	0.007926	0.006692	0.006596
Barr $h_{\pi^+}$	0.000000	-0.147475	-0.148481	-0.148059	0.147475	0.148481	0.148059
Barr $i_{\pi^+}$	0.000000	0.475448	0.513393	0.521626	-0.475448	-0.513393	-0.521626
Barr $y_{K^+}$	0.000000	0.076176	0.062893	0.057548	-0.076176	-0.062893	-0.057548
$\theta_{23}[\circ]$	47.504700	48.117185	47.918758	48.010986	-0.612485	-0.414058	-0.506286
$\Delta m_{31}^2 [\text{eV}^2]$	0.002475	0.002454	0.002454	0.002455	0.000020	0.000021	0.000019
DIS	0.000000	-0.248709	-0.223302	-0.215666	0.248709	0.223302	0.215666
$N_\nu$	1.000000	0.889149	0.889055	0.889559	0.110851	0.110945	0.110441
$ U_{\tau 4} ^2$	0.100000	0.003019	0.080494	0.106141	0.096981	0.019506	-0.006141
$\epsilon_{\text{DOM}}$	1.000000	1.021984	1.017789	1.016689	-0.021984	-0.017789	-0.016689
hole ice $p_0$	0.101569	-0.161341	-0.161051	-0.160129	0.262910	0.262620	0.261698
hole ice $p_1$	-0.049344	-0.073701	-0.075596	-0.076261	0.024357	0.026252	0.026917
ice absorption	1.000000	0.943261	0.942463	0.942000	0.056739	0.057537	0.058000
ice scattering	1.050000	0.986152	0.989289	0.989438	0.063848	0.060711	0.060562
$N_{\text{bfr}}$	0.000000	0.746684	0.740255	0.736215	-0.746684	-0.740255	-0.736215
$M_{A,\text{QE}}$	0.000000	-0.170528	-0.128150	-0.120345	0.170528	0.128150	0.120345
$M_{A,\text{res}}$	0.000000	-0.125855	-0.080875	-0.070716	0.125855	0.080875	0.070716

sort these by type of nuisance parameter?

### C.2 Best Fit Parameters and Limits

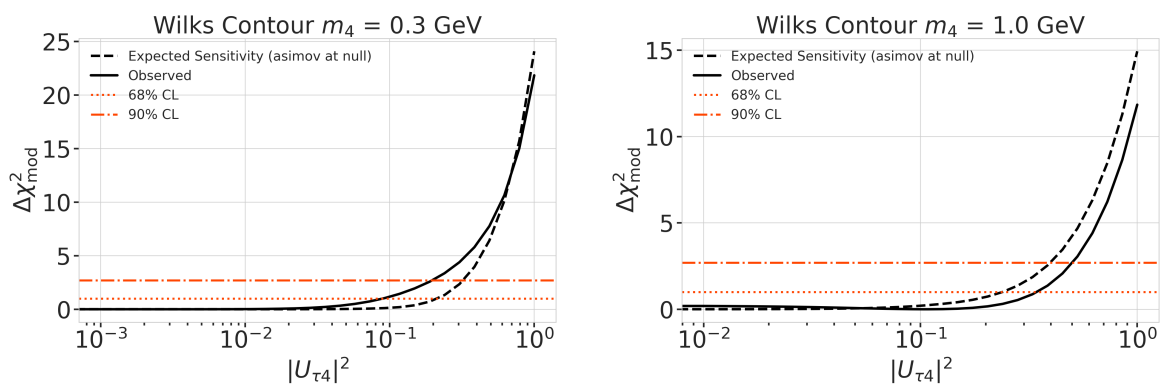


Figure C.1: xx

# Bibliography

Here are the references in citation order.

- [1] C. N. Yang and R. L. Mills. "Conservation of Isotopic Spin and Isotopic Gauge Invariance". In: *Physical Review* 96.1 (Oct. 1954), pp. 191–195. doi: [10.1103/PhysRev.96.191](https://doi.org/10.1103/PhysRev.96.191) (cited on page 1).
- [2] S. Weinberg. "A Model of Leptons". In: *Phys. Rev. Lett.* 19 (21 Nov. 1967), pp. 1264–1266. doi: [10.1103/PhysRevLett.19.1264](https://doi.org/10.1103/PhysRevLett.19.1264) (cited on page 1).
- [3] S. L. Glashow. "Partial-symmetries of weak interactions". In: *Nuclear Physics* 22.4 (Feb. 1961), pp. 579–588. doi: [10.1016/0029-5582\(61\)90469-2](https://doi.org/10.1016/0029-5582(61)90469-2) (cited on page 1).
- [4] R. Jackiw. "Physical Formulations: Elementary Particle Theory. Relativistic Groups and Analyticity. Proceedings of the eighth Nobel Symposium, Aspenäsgården, Lerum, Sweden, May 1968. Nils Svartholm, Ed. Interscience (Wiley), New York, and Almqvist and Wiksell, Stockholm, 1969. 400 pp., illus. \$31.75." In: *Science* 168.3936 (1970), pp. 1196–1197. doi: [10.1126/science.168.3936.1196.b](https://doi.org/10.1126/science.168.3936.1196.b) (cited on page 1).
- [5] P. Higgs. "Broken symmetries, massless particles and gauge fields". In: *Physics Letters* 12.2 (1964), pp. 132–133. doi: [https://doi.org/10.1016/0031-9163\(64\)91136-9](https://doi.org/10.1016/0031-9163(64)91136-9) (cited on page 1).
- [6] M. Gell-Mann. "A Schematic Model of Baryons and Mesons". In: *Resonance* 24 (1964), pp. 923–925 (cited on page 1).
- [7] G. Zweig. "An SU(3) model for strong interaction symmetry and its breaking. Version 2". In: *DEVELOPMENTS IN THE QUARK THEORY OF HADRONS. VOL. 1. 1964 - 1978*. Ed. by D. B. Lichtenberg and S. P. Rosen. Feb. 1964, pp. 22–101 (cited on page 1).
- [8] D. J. Gross and F. Wilczek. "Ultraviolet Behavior of Non-Abelian Gauge Theories". In: *PRL* 30.26 (June 1973), pp. 1343–1346. doi: [10.1103/PhysRevLett.30.1343](https://doi.org/10.1103/PhysRevLett.30.1343) (cited on page 1).
- [9] C. Giunti and C. W. Kim. *Fundamentals of Neutrino Physics and Astrophysics*. Oxford University Press, Mar. 2007 (cited on page 1).
- [10] M. D. Schwartz. *Quantum Field Theory and the Standard Model*. Cambridge University Press, 2013 (cited on page 1).
- [11] A. Terliuk. "Measurement of atmospheric neutrino oscillations and search for sterile neutrino mixing with IceCube DeepCore". PhD thesis. Berlin, Germany: Humboldt-Universität zu Berlin, Mathematisch-Naturwissenschaftliche Fakultät, 2018. doi: [10.18452/19304](https://doi.org/10.18452/19304) (cited on pages 3, 8).
- [12] M. Thomson. *Modern particle physics*. Cambridge [u.a.]: Cambridge University Press, 2013, XVI, 554 S. (Cited on page 3).
- [13] R. Davis, D. S. Harmer, and K. C. Hoffman. "Search for Neutrinos from the Sun". In: *Phys. Rev. Lett.* 20 (21 May 1968), pp. 1205–1209. doi: [10.1103/PhysRevLett.20.1205](https://doi.org/10.1103/PhysRevLett.20.1205) (cited on page 4).
- [14] Y. Fukuda et al. "Evidence for Oscillation of Atmospheric Neutrinos". In: *Phys. Rev. Lett.* 81 (8 Aug. 1998), pp. 1562–1567. doi: [10.1103/PhysRevLett.81.1562](https://doi.org/10.1103/PhysRevLett.81.1562) (cited on page 4).
- [15] Q. R. Ahmad and other. "Direct Evidence for Neutrino Flavor Transformation from Neutral-Current Interactions in the Sudbury Neutrino Observatory". In: *Phys. Rev. Lett.* 89 (1 June 2002), p. 011301. doi: [10.1103/PhysRevLett.89.011301](https://doi.org/10.1103/PhysRevLett.89.011301) (cited on page 4).
- [16] M. Tanabashi et al. "Review of Particle Physics". In: *Phys. Rev. D* 98 (3 Aug. 2018), p. 030001. doi: [10.1103/PhysRevD.98.030001](https://doi.org/10.1103/PhysRevD.98.030001) (cited on pages 4, 6, 9).
- [17] M. Aker et al. "Direct neutrino-mass measurement with sub-electronvolt sensitivity". In: *Nature Phys.* 18.2 (2022), pp. 160–166. doi: [10.1038/s41567-021-01463-1](https://doi.org/10.1038/s41567-021-01463-1) (cited on page 4).

- [18] S. Alam et al. "Completed SDSS-IV extended Baryon Oscillation Spectroscopic Survey: Cosmological implications from two decades of spectroscopic surveys at the Apache Point Observatory". In: *Phys. Rev. D* 103 (8 Apr. 2021), p. 083533. doi: [10.1103/PhysRevD.103.083533](https://doi.org/10.1103/PhysRevD.103.083533) (cited on page 4).
- [19] N. Aghanim et al. "Planck2018 results: VI. Cosmological parameters". In: *Astronomy & Astrophysics* 641 (Sept. 2020), A6. doi: [10.1051/0004-6361/201833910](https://doi.org/10.1051/0004-6361/201833910) (cited on page 4).
- [20] P. Coloma et al. "GeV-scale neutrinos: interactions with mesons and DUNE sensitivity". In: *Eur. Phys. J. C* 81.1 (2021), p. 78. doi: [10.1140/epjc/s10052-021-08861-y](https://doi.org/10.1140/epjc/s10052-021-08861-y) (cited on pages 6, 11, 13).
- [21] M. Honda et al. "Atmospheric neutrino flux calculation using the NRLMSISE-00 atmospheric model". In: *Phys. Rev. D* 92 (2 July 2015), p. 023004. doi: [10.1103/PhysRevD.92.023004](https://doi.org/10.1103/PhysRevD.92.023004) (cited on page 7).
- [22] A. Fedynitch et al. "Calculation of conventional and prompt lepton fluxes at very high energy". In: *European Physical Journal Web of Conferences*. Vol. 99. European Physical Journal Web of Conferences. Aug. 2015, p. 08001. doi: [10.1051/epjconf/20159908001](https://doi.org/10.1051/epjconf/20159908001) (cited on page 7).
- [23] J. A. Formaggio and G. P. Zeller. "From eV to EeV: Neutrino cross sections across energy scales". In: *Rev. Mod. Phys.* 84 (3 Sept. 2012), pp. 1307–1341. doi: [10.1103/RevModPhys.84.1307](https://doi.org/10.1103/RevModPhys.84.1307) (cited on page 9).
- [24] S. Bilenky and B. Pontecorvo. "Lepton mixing and neutrino oscillations". In: *Physics Reports* 41.4 (1978), pp. 225–261. doi: [10.1016/0370-1573\(78\)90095-9](https://doi.org/10.1016/0370-1573(78)90095-9) (cited on page 8).
- [25] P. A. M. Dirac. "The Quantum Theory of the Emission and Absorption of Radiation". In: *Proceedings of the Royal Society of London Series A* 114.767 (Mar. 1927), pp. 243–265. doi: [10.1098/rspa.1927.0039](https://doi.org/10.1098/rspa.1927.0039) (cited on page 9).
- [26] T. Yanagida. "Horizontal Symmetry and Masses of Neutrinos". In: *Progress of Theoretical Physics* 64.3 (Sept. 1980), pp. 1103–1105. doi: [PTP.64.1103](https://doi.org/10.1143/PTP.64.1103) (cited on page 10).
- [27] P. Astier et al. "Search for heavy neutrinos mixing with tau neutrinos". In: *Phys. Lett. B* 506 (2001), pp. 27–38. doi: [10.1016/S0370-2693\(01\)00362-8](https://doi.org/10.1016/S0370-2693(01)00362-8) (cited on page 11).
- [28] R. Acciari et al. "New Constraints on Tau-Coupled Heavy Neutral Leptons with Masses mN=280–970 MeV". In: *Phys. Rev. Lett.* 127.12 (2021), p. 121801. doi: [10.1103/PhysRevLett.127.121801](https://doi.org/10.1103/PhysRevLett.127.121801) (cited on page 11).
- [29] J. Orloff, A. N. Rozanov, and C. Santoni. "Limits on the mixing of tau neutrino to heavy neutrinos". In: *Phys. Lett. B* 550 (2002), pp. 8–15. doi: [10.1016/S0370-2693\(02\)02769-7](https://doi.org/10.1016/S0370-2693(02)02769-7) (cited on page 11).
- [30] I. Boiarska et al. "Blast from the past: constraints from the CHARM experiment on Heavy Neutral Leptons with tau mixing". In: (July 2021) (cited on page 11).
- [31] P. Abreu et al. "Search for neutral heavy leptons produced in Z decays". In: *Z. Phys. C* 74 (1997). [Erratum: *Z.Phys.C* 75, 580 (1997)], pp. 57–71. doi: [10.1007/s002880050370](https://doi.org/10.1007/s002880050370) (cited on page 11).
- [32] P. Coloma et al. "Double-Cascade Events from New Physics in Icecube". In: *Phys. Rev. Lett.* 119.20 (2017), p. 201804. doi: [10.1103/PhysRevLett.119.201804](https://doi.org/10.1103/PhysRevLett.119.201804) (cited on pages 10, 11).
- [33] P. Coloma. "Icecube/DeepCore tests for novel explanations of the MiniBooNE anomaly". In: *Eur. Phys. J. C* 79.9 (2019), p. 748. doi: [10.1140/epjc/s10052-019-7256-8](https://doi.org/10.1140/epjc/s10052-019-7256-8) (cited on page 11).
- [34] R. Abbasi et al. "Measurement of Astrophysical Tau Neutrinos in IceCube's High-Energy Starting Events". In: *arXiv e-prints* (Nov. 2020) (cited on page 15).
- [35] M. Usner. "Search for Astrophysical Tau-Neutrinos in Six Years of High-Energy Starting Events in the IceCube Detector". PhD thesis. Berlin, Germany: Humboldt-Universität zu Berlin, Mathematisch-Naturwissenschaftliche Fakultät, 2018. doi: [10.18452/19458](https://doi.org/10.18452/19458) (cited on page 15).
- [36] P. Hallen. "On the Measurement of High-Energy Tau Neutrinos with IceCube". MA thesis. Aachen, Germany: RWTH Aachen University, 2013 (cited on page 15).
- [37] N. Whitehorn, J. van Santen, and S. Lafebre. "Penalized splines for smooth representation of high-dimensional Monte Carlo datasets". In: *Computer Physics Communications* 184.9 (2013), pp. 2214–2220. doi: <https://doi.org/10.1016/j.cpc.2013.04.008> (cited on page 15).
- [38] M. G. Aartsen et al. "Energy Reconstruction Methods in the IceCube Neutrino Telescope". In: *JINST* 9 (2014), P03009. doi: [10.1088/1748-0221/9/03/P03009](https://doi.org/10.1088/1748-0221/9/03/P03009) (cited on page 15).

- [39] R. Abbasi et al. "Low energy event reconstruction in IceCube DeepCore". In: *Eur. Phys. J. C* 82.9 (2022), p. 807. doi: [10.1140/epjc/s10052-022-10721-2](https://doi.org/10.1140/epjc/s10052-022-10721-2) (cited on page 16).
- [40] S. Yu and J. Micallef. "Recent neutrino oscillation result with the IceCube experiment". In: *38th International Cosmic Ray Conference*. July 2023 (cited on page 28).
- [41] M. G. Aartsen et al. "Computational techniques for the analysis of small signals in high-statistics neutrino oscillation experiments". In: *Nucl. Instrum. Meth. A* 977 (2020), p. 164332. doi: [10.1016/j.nima.2020.164332](https://doi.org/10.1016/j.nima.2020.164332) (cited on page 28).
- [42] <https://github.com/icecube/pisa> (cited on page 28).
- [43] J. Evans et al. "Uncertainties in atmospheric muon-neutrino fluxes arising from cosmic-ray primaries". In: *Phys. Rev. D* 95 (2 Jan. 2017), p. 023012. doi: [10.1103/PhysRevD.95.023012](https://doi.org/10.1103/PhysRevD.95.023012) (cited on page 30).
- [44] J. Feintzeig. "Searches for Point-like Sources of Astrophysical Neutrinos with the IceCube Neutrino Observatory". PhD thesis. University of Wisconsin, Madison, Jan. 2014 (cited on page 30).
- [45] N. Kulacz. "In Situ Measurement of the IceCube DOM Efficiency Factor Using Atmospheric Minimum Ionizing Muons". MA thesis. University of Alberta, 2019 (cited on page 30).
- [46] R. S. Nickerson. "Confirmation Bias: A Ubiquitous Phenomenon in Many Guises". In: *Review of General Psychology* 2 (1998), pp. 175–220 (cited on page 31).
- [47] H. Dembinski et al. *scikit-hep/minuit: v2.17.0*. Version v2.17.0. Sept. 2022. doi: [10.5281/zenodo.7115916](https://doi.org/10.5281/zenodo.7115916) (cited on page 31).
- [48] F. James and M. Roos. "Minuit: A System for Function Minimization and Analysis of the Parameter Errors and Correlations". In: *Comput. Phys. Commun.* 10 (1975), pp. 343–367. doi: [10.1016/0010-4655\(75\)90039-9](https://doi.org/10.1016/0010-4655(75)90039-9) (cited on page 31).
- [49] S. S. Wilks. "The Large-Sample Distribution of the Likelihood Ratio for Testing Composite Hypotheses". In: *The Annals of Mathematical Statistics* 9.1 (1938), pp. 60–62. doi: [10.1214/aoms/1177732360](https://doi.org/10.1214/aoms/1177732360) (cited on page 33).